AD-A065 443 IOWA INST OF HYDRAULIC RESEARCH IOWA CITY F/G 20/4
AN ANALYTICAL SOLUTION OF THE THICK AXISYMMETRIC TURBULENT BOUN--ETC(U)
DEC 78 N DENLI N00014-75-C-0273
UNCLASSIFIED NL

1 OF 2
AD A065443

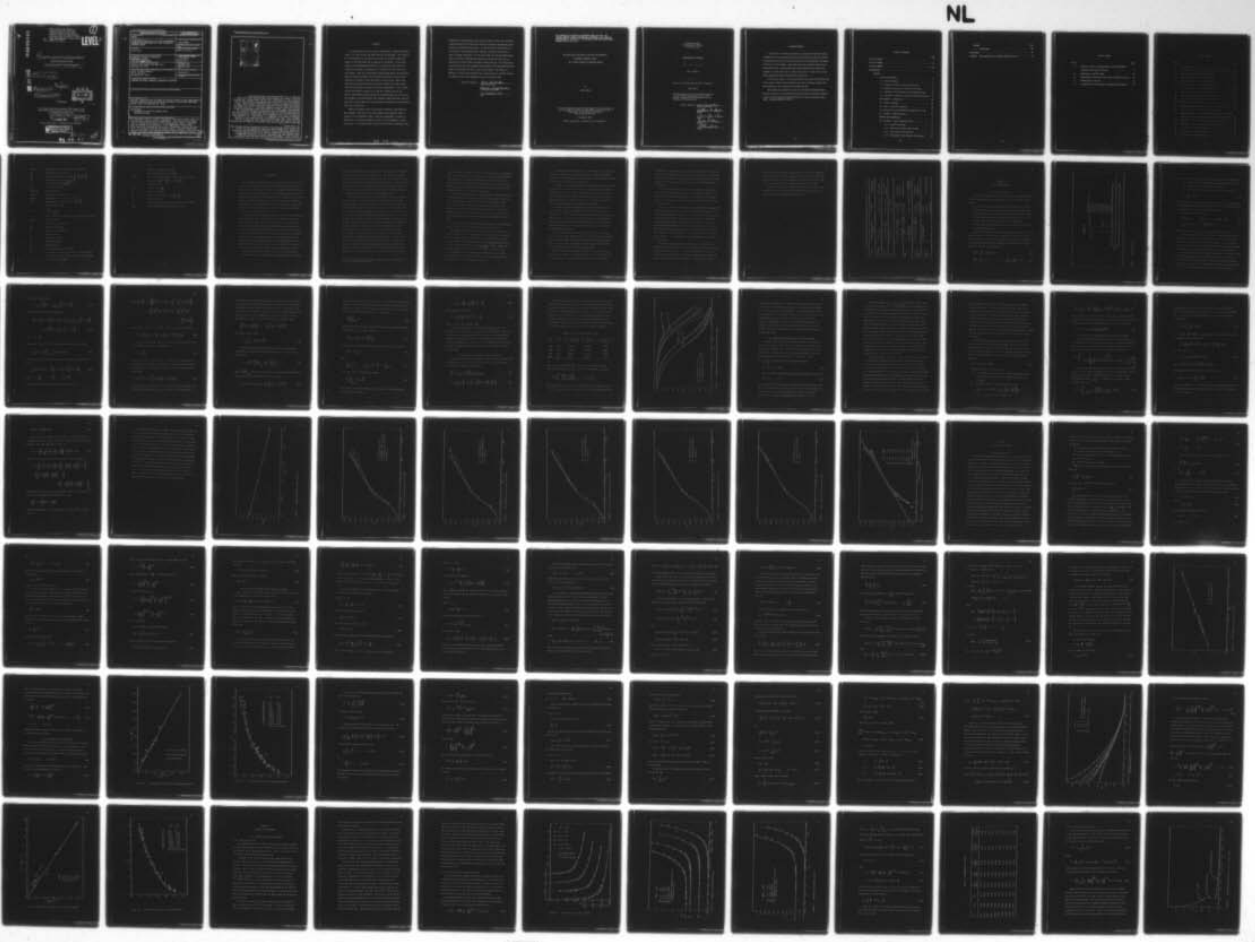

This research was partially supported under the Naval Sea Systems Command General Hydromechanics Research (GHR) Program administered by the David W. Taylor Naval Ship R&D Center under Contract (15) N00014-75-C-0273

(1) LEVEL II

(6) AN ANALYTICAL SOLUTION OF THE THICK AXISYMMETRIC TURBULENT BOUNDARY LAYER ON A LONG CYLINDER OF CONSTANT RADIUS.

(9) Final rept.,

by

(10) Nuray Denli

(16) SR02301

(17) SR02301 01

An Abstract

Of a thesis submitted in partial fulfillment of the requirements for the degree of Doctor of Philosophy in Mechanics and Hydraulics in the Graduate College of The University of Iowa

(11) December, 1978

(12) 109 p.

Thesis supervisor: Professor Louis Landweber

188 300 /B

SECURITY CLASSIFICATION OF THIS PAGE *(When Data Entered)*

REPORT DOCUMENTATION PAGE

READ INSTRUCTIONS BEFORE COMPLETING FORM

1. REPORT NUMBER: THESIS	2. GOVT ACCESSION NO.
3. RECIPIENT'S CATALOG NUMBER	
4. TITLE *(and Subtitle)*: AN ANALYTICAL SOLUTION OF THE THICK AXISYMMETRIC TURBULENT BOUNDARY LAYER ON A LONG CYLINDER OF CONSTANT RADIUS	5. TYPE OF REPORT & PERIOD COVERED: FINAL/THESIS
	6. PERFORMING ORG. REPORT NUMBER: None
7. AUTHOR(s): Nuray Denli	8. CONTRACT OR GRANT NUMBER(s): N00014-75-C-0273
9. PERFORMING ORGANIZATION NAME AND ADDRESS: Institute of Hydraulic Research, ~~University of~~ Iowa, Iowa City, ~~Iowa~~ 52242	10. PROGRAM ELEMENT, PROJECT, TASK AREA & WORK UNIT NUMBERS: 61153N R02301; SR 023 01 01
11. CONTROLLING OFFICE NAME AND ADDRESS: David W. Taylor Naval Ship R&D Center, Bethesda, Md 20084	12. REPORT DATE: December 1978
	13. NUMBER OF PAGES: 93
14. MONITORING AGENCY NAME & ADDRESS *(if different from Controlling Office)*: Office of Naval Research, 800 N. Quincy St, Arlington, Va 22217	15. SECURITY CLASS. *(of this report)*: Unclassified
	15a. DECLASSIFICATION/DOWNGRADING SCHEDULE

16. DISTRIBUTION STATEMENT *(of this Report)*

APPROVED FOR PUBLIC RELEASE: DISTRIBUTION UNLIMITED

17. DISTRIBUTION STATEMENT *(of the abstract entered in Block 20, if different from Report)*

18. SUPPLEMENTARY NOTES

Partially supported under the Naval Sea Systems Command General Hydromechanics Research (GHR) Program administered by the David W. Taylor Naval Ship R&D Center, Code 1505, Bethesda, Md 20084

19. KEY WORDS *(Continue on reverse side if necessary and identify by block number)*

GHR Program
Axisymmetric Turbulent Boundary Layer
Circular Cylinder

20. ABSTRACT *(Continue on reverse side if necessary and identify by block number)*

Two similarity laws for a thick, axisymmetric, turbulent boundary layer on a long circular cylinder have been established. The validity of the assumption of constant-stress moment in the law-of-the-wall region is analyzed under the assumption of similarity. A new logarithmic mixing length, which takes into consideration the effect of transverse curvature on turbulence, is proposed for the law-of-the-wall region. With this logarithmic mixing-length model, the mean-flow momentum equation yeilds a law-of-the-wall relation in terms of the exponential integral in the logarithmic portion of

next pg.

DD FORM 1 JAN 73 1473 EDITION OF 1 NOV 65 IS OBSOLETE
S/N 0102-LF-014-6601

188300

SECURITY CLASSIFICATION OF THIS PAGE *(When Data Entered)*

the inner layer. Comparisons with available data and other proposed relations reveal that this logarithmic law gives a definite improvement. Also a mathematical explanation is given as to why the cylinder data do not deviate appreciably from the classical two-dimensional law-of-the-wall, even though it is observed that the turbulent characteristics, such as the size of large eddies and the turbulent intensities are much smaller than for a flat plate.

When the boundary layer is very thick relative to the radius of the cylinder, the flow in the outer region of the boundary layer is similar to an axisymmetric wake. With this assumption, a velocity-defect law is derived, analogous to that for an axisymmetric, turbulent wake. It is assumed that the velocity defect has a separable form. Depending on the modeling of the turbulent shear stress, the mean-flow momentum equation in conjunction with the similarity assumption, gives different differential equations. An eddy-viscosity model leads to a second-order linear differential equation, solutions of which are known as Kummer functions. On the other hand, the mixing-length model gives a nonlinear differential equation for which the solution is obtained in terms of semi-convergent infinite series. The comparisons of the results with the available data indicate that the eddy-viscosity model is preferable to that of the mixing length. The former is applied to compute the boundary-layer charactersitcis, and the results are shown to be in good agreement with the available data.

ABSTRACT

Two similarity laws for a thick, axisymmetric, turbulent boundary layer on a long circular cylinder have been established. The validity of the assumption of constant-stress moment in the law-of-the-wall region is analyzed under the assumption of similarity. A new logarithmic mixing length, which takes into consideration the effect of transverse curvature on turbulence, is proposed for the law-of-the-wall region. With this logarithmic mixing-length model, the mean-flow momentum equation yields a law-of-the-wall relation in terms of the exponential integral in the logarithmic portion of the inner layer. Comparisons with available data and other proposed relations reveal that this logarithmic law gives a definite improvement. Also a mathematical explanation is given as to why the cylinder data do not deviate appreciably from the classical two-dimensional law of the wall, even though it is observed that the turbulent characteristics, such as the size of large eddies and the turbulent intensities are much smaller than for a flat plate.

When the boundary layer is very thick relative to the radius of the cylinder, the flow in the outer region of the boundary layer is similar to an axisymmetric wake. With this assumption, a velocity-defect law is derived, analogous to that for an axisymmetric, turbulent wake. It is assumed that the velocity defect has a separable form.

Depending on the modeling of the turbulent shear stress, the mean-flow momentum equation in conjunction with the similarity assumption, gives different differential equations. An eddy-viscosity model leads to a second-order linear differential equation, solutions of which are known as Kummer functions. On the other hand, the mixing-length model gives a nonlinear differential equation for which the solution is obtained in terms of semi-convergent infinite series. The comparisons of the results with the available data indicate that the eddy-viscosity model is preferable to that of the mixing length. The former is applied to compute the boundary-layer characteristics, and the results are shown to be in good agreement with the available data.

Abstract approved: Louis Landweber
Thesis supervisor

Professor, Energy Division
Title and department

20 September 1978
Date

THIS RESEARCH WAS PARTIALLY SUPPORTED UNDER THE NAVAL SEA SYSTEMS COMMAND GENERAL HYDROMECHANICS RESEARCH (GHR) PROGRAM ADMINISTERED BY THE DAVID W. TAYLOR NAVAL SHIP R&D CENTER UNDER CONTRACT N00014-75-C-0273

AN ANALYTICAL SOLUTION OF THE THICK AXISYMMETRIC TURBULENT BOUNDARY LAYER ON A LONG CYLINDER OF CONSTANT RADIUS

by

Nuray Denli

A thesis submitted in partial fulfillment of the requirements for the degree of Doctor of Philosophy in Mechanics and Hydraulics in the Graduate College of The University of Iowa

December, 1978

Thesis supervisor: Professor Louis Landweber

Graduate College
The University of Iowa
Iowa City, Iowa

CERTIFICATE OF APPROVAL

PH.D. THESIS

This is to certify that the Ph.D. thesis of

Nuray Denli

has been approved by the Examining Committee
for the thesis requirement for the Ph.D.
degree in Mechanics and Hydraulics at the
December, 1978 graduation.

Thesis committee: Louis Landweber
Thesis supervisor

William W. Sayre
Member

Member

Kendall E. Atkinson
Member

B R Ramaprian
Member

ACKNOWLEDGEMENTS

I would like to thank and express my gratitude to Professor Louis Landweber who first proposed the study and devoted his time for helpful discussions and offered continuous guidance and encouragement throughout the course of this study. I also appreciate his critical review of the thesis manuscript. Without his help, this thesis would not have been possible. I would also like to thank Professor V.C. Patel for his many useful suggestions and the materials he supplied.

Last but not least, I owe my gratitude to my mother Talia Denli and to my sisters Tülay, Gülay and Hülya for their continuous support and encouragement at all stages of my academic career.

The project was supported in part by the General Hydromechanics Research Program of the Naval Ship Systems Command, technically administered by the David Taylor Naval Ship Research and Development Center, under Contract N00014-75-C-0273.

TABLE OF CONTENTS

LIST OF TABLES

LIST OF FIGURES

LIST OF SYMBOLS

a	Radius of cylinder
a^*	Frictional Reynolds number based on cylinder radius $\left(= \frac{au_\tau}{\nu}\right)$
b	Constant in Eq. (74)
B, $B(a^*)$ $B'(a^*)$, $B_r(a^*)$	Notations generally used for the intercept of the logarithmic law of the inner layer
$E_i(x)$	Exponential integral
f, F	"function of"
${}_1F_1(b,1,z)$	Kummer function
m	Constant in Eq. (66)
$M(b,1,z)$	Another notation for the Kummer function ${}_1F_1(b,1,z)$
ℓ	Mixing length
ℓ^*	Nondimensional mixing length $\left(= \frac{\ell u_\tau}{\nu}\right)$
$\bar{\ell}$	Nondimensional mixing length $\left(= \frac{\ell}{a}\right)$
$\bar{r}$	Nondimensional radial distance $\left(= \frac{r}{a}\right)$
$\bar{r}_c$	Intersection point of the law-of-the-wall and the velocity-defect law
R	Nondimensional boundary layer thickness $\left(= \frac{\delta + a}{a}\right)$
Re_a	Reynolds number based on free-stream velocity and cylinder radius $\left(= \frac{aU_e}{\nu}\right)$
R_x	Reynolds number based on free-stream velocity and longitudinal coordinate x $\left(= \frac{xU_e}{\nu}\right)$

(u,v)	Longitudinal and radial velocity components
u_d	Defect velocity $(= U_e - u)$
$\bar{u}_d$	Nondimensional defect velocity $\left(= \frac{u_d}{U_e}\sqrt{Re_a}\right)$
u^*	Nondimensional velocity $\left(= \frac{u}{u_\tau}\right)$
u_τ	Friction velocity $\left(= \sqrt{\frac{\tau_w}{\rho}}\right)$
U_e	Free-stream velocity
$U(b,1,z)$	Kummer function
(x,r)	Cylindrical coordinates
(x,y)	Cylindrical coordinates $(y = r - a)$
y^*	Nondimensional radial distance $\left(= \frac{yu_\tau}{\nu}\right)$
α	Constant in Eq. (64)
β	$\beta \equiv \frac{U_e}{u} \frac{1}{\sqrt{2}\ Re_a^{3/4}}$
γ	Euler's constant = 0.5772...; a constant in Eq. (125)
$\Gamma(b)$	Gamma function
δ	Boundary-layer thickness
δ_1	Displacement length
δ^*	Displacement thickness
ε	Eddy viscosity
ζ	A variable $(= \eta/\alpha)$
θ	Momentum thickness
θ_1	Momentum length
κ	Von Kármán's constant (=0.418)
λ	A constant in mixing-length model given by Eq. (8); a constant in eddy-viscosity model given by Eq. (66)
λ_ℓ	A constant in Eq. (120)

μ	Dynamic viscosity of the fluid
ν	Kinematic viscosity of the fluid
(ξ,η)	Nondimensional longitudinal and radial coordinates, respectively $\left(\xi^2 = \frac{x/a}{Re_a}, \quad \eta = \frac{y + a}{\delta + a}\right)$
ρ	Fluid density
σ,σ'	$\sigma \equiv \frac{U_e}{u}, \quad \sigma' = \frac{d\sigma}{dR_x}$
τ	Total shear stress
τ^+	Nondimensional shear stress $\left(= \frac{\tau}{\tau_w}\right)$
τ_w	Wall-shear stress
χ	A function defining the velocity defect in Eq. (52)
$\psi(b)$	Logarithmic derivative of gamma function

INTRODUCTION

A turbulent boundary layer on a transversely curved surface has a different structure from that of a flat-plate boundary layer if the boundary-layer thickness δ is of the same or higher order than that of a typical transverse dimension of the body. This transverse-curvature effect is of importance in computations of the boundary layer near the tail of a body of revolution, in estimating the surface resistance of ship models, or other three-dimensional elongated bodies. Since thin boundary-layer approximations are not valid, these so-called thick boundary layers need special treatment.

The growth of the turbulent boundary layer on a circular cylinder of constant radius is a special case of the problem of transverse-curvature effect, since the pressure gradient is almost zero everywhere and there is no strong interaction between the boundary layer and the external flow. This problem has been studied in the past both by experimental and theoretical methods, because of many engineering applications in hydrodynamics, aerodynamics, instrumentation and textile engineering, and also, because of the simple geometry which isolates the effect of transverse curvature from that of the longitudinal radius of curvature of other elongated axisymmetric bodies.

Although the effect of transverse curvature in laminar, axisymmetric boundary layers has been well established by Seban and Bond

[1], Kelly [2] and by Glauert and Lighthill [3], much less analytical work has been done for the turbulent case. In 1949, Landweber [4] investigated the transverse-curvature effect by using the 1/7-th power-law velocity profile and the Blasius skin-friction law. He showed that, at a given value of momentum-thickness Reynolds number, the skin friction on the cylinder was greater than that of a flat plate, and that the boundary-layer thickness was correspondingly smaller.

Most of the investigators in this area were concerned only with the inner layer, particularly with the logarithmic portion of the law of the wall. They all assumed that the classical two-dimensional law of the wall had to be modified. Some of them tried to modify the constants of the two-dimensional logarithmic law, and others modified the argument of the function, but not the function itself. For example, in 1957, Richmond [5] obtained a law of the wall for the axisymmetric boundary layer by using Coles' streamline hypothesis in the region near the wall where he assumed that mean flow is dominated by the wall. Richmond proposed an expression for the nondimensional velocity $u^* = u/u_\tau^\dagger$ as a function of the argument $y^*(1 + y/2a)$. He, then, obtained the logarithmic law simply by replacing the argument of the two-dimensional logarithmic law by this new argument. In 1967, Rao [6] showed that the viscous-sublayer relation is not linear for axisymmetric flows, but is given by $u^* = a^* \ln \frac{r}{a}$. With y^* replaced by $a^* \ln \frac{r}{a}$ in $u^* = \frac{1}{\kappa} \ln y^* + B$, he proposed a different form for the

---

† Symbols are defined in the "list of symbols" and in the subsequent chapters where they first occur.

law of the wall, in which he kept the constants of the two-dimensional law. Later, however, the experiments of Rao and Keshavan [7] showed that the universal constants of a flat-plate boundary layer are "functions" of Re_a and a^* for axisymmetric flows. On the other hand, Yu [8] and Chin et al. [9] kept the form of the two-dimensional logarithmic law but tried to modify the constants.

Other work done in this area employed closure models of two-dimensional flows and the assumption of constant stress moment in the law-of-the-wall region. In 1963, Sparrow, Eckert and Minkowycz [10] analyzed the turbulent velocity and thermal boundary layers on a cylinder of constant radius by using Deissler's eddy-viscosity model. In 1972, Patel [11] obtained a solution for the inner layer by using a two-dimensional, mixing-length model given by Landweber and Poreh [12].

Table I.1 summarizes the velocity distributions in the logarithmic portion of the law of the wall proposed by various authors.

Although the boundary layer on a long slender rod, when $\delta/a >> 1$, is almost all a wake-like flow, very little attention has been paid to the wake portion of the boundary layer. Rao and Keshavan [7] tried to find a similarity variable for the velocity-defect region by trial and error. They found that the velocity defect $\frac{U_e - u}{u_\tau}$ yields similarity in terms of the variable $r^* = \frac{(a + y)u_\tau}{\nu}$, based on their experimental data. On the other hand, Yu [8] and Chin et al. [9] presented their measurements in classical two-dimensional defect-law coordinates and tried to adjust the constants.

In 1972, White [13] approached the problem with a simple integral analysis in which he assumed that the law of the wall suggested by Rao [6] is valid throughout the boundary layer. Thus, the wake portion of the boundary layer was not considered.

In 1970, Cebeci [14] solved the turbulent boundary-layer equations by an implicit finite-difference method, applied after the momentum equations had been linearized. In his treatment, Cebeci, used an eddy-viscosity model of thin, two-dimensional boundary layers which ignores the effect of transverse curvature on turbulence. However, Cebeci's solution is the only complete one available.

In 1976, Afzal and Narasimha [15] studied the problem at large values of the frictional Reynolds number based on the radius of cylinder a, $a^* = \frac{au_\tau}{\nu}$, with the boundary-layer thickness δ of order a. They used the equations of the mean flow and the method of matched asymptotic expansions to show that the flow can be described by the inner- and outer-layer concepts that are used in two-dimensional turbulent boundary layers.

Some of the researchers, however, did only experimental work; namely: Yasuhara [16], Willmarth and Young [17] and Willmarth, Winkel, Bogar and Sharma [18]. But the only measurement of turbulent quantities (except the wall-pressure fluctuations measured by Willmarth et al. [17,18]) are given by Afzal and Singh [19].

Although a large number of measurements for the mean velocity profiles are available, the similarity laws for the axisymmetric turbulent flow along a circular cylinder have not as yet been well

established. Hence, this study is mainly concerned with the determination of the similarity laws by using the mean-flow momentum equations and closure relations for the Reynolds stress distributions, and their application to improve the calculations of the boundary-layer characteristics.

It is well-known that, for axisymmetric flows, the total shear stress is not constant, but that the stress moment, $r\tau$, may be assumed to be constant in the law-of-the-wall region. The validity of this assumption is analyzed in conjunction with similarity of the flow, in Chapter 1.

The measurements of Willmarth et al. [17,18], Afzal and Singh [19] and Patel, Nakayama and Damian [20] reveal that the transverse-curvature affects turbulence directly. The results indicate that turbulence intensities, and the size of the large eddies and consequently the mixing length are reduced compared to values for a flat plate. A mixing-length model which takes these characteristics into account is proposed in Chapter 1, and applied to deduce a law of the wall from the mean-flow momentum equations. The results are compared with the data of Willmarth et al. [18], and with other proposed forms of the law of the wall.

When a/δ approaches zero, the cylinder may be considered as a small vorticity-and turbulence-producing disturbance. Hence the flow may be considered to be similar to an axisymmetric wake flow. The important difference is that the drag generating the wake is not constant, but a function of the longitudinal coordinate. With these

considerations, in Chapter 2, a similarity law has been derived for the velocity-defect region, analogous to the axisymmetric turbulent wake, both by using eddy-viscosity and mixing-length concepts. The results are compared with the data of Willmarth et al. [18].

In Chapter 3, using the results of the law-of-the-wall and the velocity-defect law, an approximate method has been presented for computing the boundary-layer characteristics.

TABLE I.1 PROPOSED VELOCITY DISTRIBUTIONS IN THE LOGARITHMIC PORTION OF THE LAW OF THE WALL

Author(s)	Velocity Distribution in the Log-Region	Parameter	Closure Relation (or derivation)
Classical two-dimensional law	$u^* = \frac{1}{\kappa} \ln y^* + B$	$\kappa = 0.418$, $B = 5.45$	Overlap concept
Richmond [5] (1957)	$u^* = \frac{1}{\kappa} \ln \left[y^* \left(1 + \frac{y^*}{2a^*} \right) \right] + B$	$\kappa = 0.4$, $B = 5.10$	Coles' streamline hypothesis
Yu [8] (1958)	$u^* = \frac{1}{\kappa} \ln y^* + B_1$	$\kappa = 0.40$, $B = B(Re_a)$	
Sparrow et al. [10] (1963)	$u^* - u_1^* = \frac{\sqrt{3}}{\kappa} \left[\tan^{-1} \left(\frac{2\beta + 1}{\sqrt{3}} \right) - \tan^{-1} \left(\frac{2\beta_1 + 1}{\sqrt{3}} \right) \right] + \frac{1}{\kappa} \ln \left(\frac{\beta - 1}{\beta_1 - 1} \right) - \frac{2}{\kappa} \ln \left(\frac{\beta^2 + \beta + 1}{\beta_1^2 + \beta_1 + 1} \right)$	$\beta = \left(1 + \frac{y^*}{a^*} \right)^{1/2}$ $\beta_1 = \left(1 + \frac{y_1^*}{a^*} \right)^{1/2}$ $\kappa = 0.39$, $n = 0.109$	Near the wall $\frac{\varepsilon}{\nu} = n^2 u^* y^*$ Away from the wall $\frac{\varepsilon}{\nu} = \kappa^2 \frac{(du^*/dy^*)^3}{(d^2u^*/dy^{*2})^2}$
Rao and Keshavan [7] (1972)	$u^* = A_1 \ln \left[a^* \ln \left(1 + \frac{y^*}{a^*} \right) \right] + A_2$	$A_1 = A_1(Re_a)$ $A_2 = A_2(Re_a, a^*)$	From viscous - sublayer relation
Patel [11] (1972)	$u^* = \frac{1}{\kappa} \ln \frac{\beta - 1}{\beta + 1} + B_r^*$	$\kappa = 0.418$ $B_r^* = B_r^*(a^*)$ β same as above	$\ell^* = \kappa y^* [\tanh(\lambda^2 y^{*2})]^{1/2}$

CHAPTER 1

THE LAW OF THE WALL

1.1 General Remarks

For a thick boundary layer growing on a long, slender cylinder of constant radius, due to the simple geometry, it is generally assumed that:

i) The mean-flow streamlines remain almost parallel to the surface regardless of the relative boundary-layer thickness. This assumption implies that the normal component of the mean velocity is much smaller than the longitudinal component, that is $v \ll u$, and hence the induced pressure gradient is negligible.

ii) The magnitudes of Reynolds stresses are similar to those of a flat-plate boundary layer.

Under these assumptions, the boundary layer develops in a constant pressure field. In terms of the cylindrical coordinates (x,y) shown in Fig. 1, where x and y are the coordinates parallel and perpendicular to the axis of symmetry of the cylinder, respectively, the boundary-layer equations for the mean flow are

$$u \frac{\partial u}{\partial x} + v \frac{\partial u}{\partial y} - \frac{1}{\rho r} \frac{\partial}{\partial y} (r\tau) = 0 \tag{1}$$

$$\frac{\partial (ur)}{\partial x} + \frac{\partial}{\partial y} (rv) = 0 \quad , \qquad \text{or} \qquad r \left(\frac{\partial u}{\partial x} + \frac{\partial v}{\partial y} \right) + v = 0 \tag{2}$$

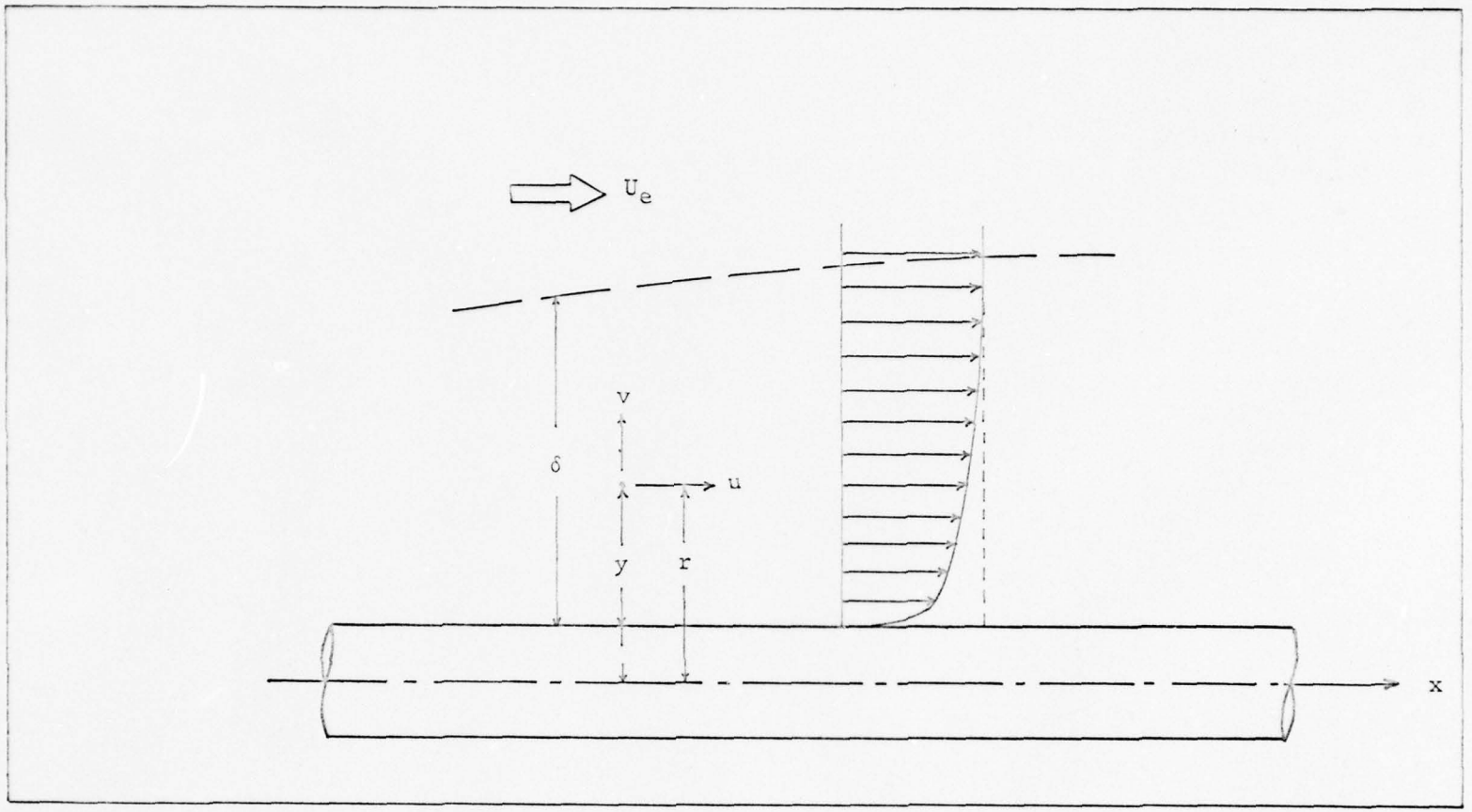

Figure 1. Definition Sketch

where $u = u(x,y)$ is the mean velocity component in the x-direction.

$v = v(x,y)$ is the mean velocity component in the y-direction.

$r = a + y$, with a the radius of the cylinder.

$\tau = \tau(x,y)$ is the total shear stress, which is given by

$$\tau = \mu \frac{\partial u}{\partial y} - \rho \overline{u'v'} \tag{3}$$

Here ρ and μ are the density and the dynamic viscosity of the fluid, and $\rho\overline{u'v'}$ is the so-called Reynolds shear stress due to the fluctuating components u' and v' of the instantaneous velocity.

The boundary conditions are

$$u(x,0) = 0 \quad , \qquad v(x,0) = 0 \quad , \qquad \tau(x,0) = \tau_w(x) \tag{4}$$

$$\lim_{y\to\infty} u(x,y) = U_e \quad , \qquad \lim_{y\to\infty} v(x,y) = 0 \tag{5}$$

where U_e is the velocity at the edge of the boundary layer.

Since it is assumed that the curvatures of the mean-flow streamlines are negligible, the interaction between the boundary layer and the external flow may be assumed to be negligible also. Therefore, once the external flow is specified, Eq. (1) and Eq. (2) can be solved by using a proper closure relationship for the Reynolds stresses.

The simplest and the most commonly used closure relations are given by the classical phenomenological theories, which relate Reynolds stresses to the mean flow through the well-known concepts of mixing length and eddy viscosity. Using the mixing-length concept, Patel[11] gives the velocity distribution in the law-of-the-wall region as

$$u^* = \int_0^{y^*} \frac{2\tau^+ \, dy^*}{1 + \{1 + 4\ell^{*2}\tau^+\}^{\frac{1}{2}}} \tag{6}$$

where $\tau^+ = \frac{\tau}{\tau_w}$, $u^* = \frac{u}{u_\tau}$, $y^* = \frac{u_\tau y}{\nu}$, $\ell^* = \frac{u_\tau \ell}{\nu}$

$$u_\tau = \sqrt{\frac{\tau_w}{\rho}} \tag{7}$$

τ_w = the shear stress at y = 0,

ℓ = mixing length.

For thin boundary layers, there are numerous formulations for the mixing-length distribution. As discussed by Patel[11], the most recent and appropriate one, given by Landweber and Poreh[12], is

$$\ell^* = \kappa y^* \sqrt{\tanh(\lambda^2 y^{*2})} \tag{8}$$

where $\kappa = 0.418$ is the Von Kármán constant,

$\lambda = \sqrt{3}/63$ is a constant given by Patel[11].

For a flat-plate boundary layer, τ^+ is assumed to be unity and Eqs. (6) and (8) give the law of the wall. For an axisymmetric, turbulent boundary layer, however, it is well known that the total stress, τ, does not remain constant in the law-of-the-wall region, although, under certain conditions, the stress moment ($r\tau$) can be assumed to be constant and equal to ($a\tau_w$).

1.2 Analysis of Shear-Stress Distribution

It is usually assumed that, in a turbulent flow along a smooth wall, the velocity distribution, in the part of the boundary layer

nearest the wall, depends upon only the density, viscosity of the fluid and the wall shear stress. Dimensional analysis, applied to the variables (u, y, a, τ_w, ρ, ν), then gives the functional relation

$$u^* = f(y^*, a^*) \tag{9}$$

Assuming that the functional relation given by Eq. (9) holds for a thick axisymmetric boundary layer on a circular cylinder of constant radius, Eqs. (1), (2) and (9) give an expression for τ^+ as follows:

$$\frac{\partial u}{\partial x} = \frac{\partial}{\partial x}\left[u_\tau\, f(y^*, a^*)\right] = \frac{du_\tau}{dx} f + u_\tau \left[\frac{\partial f}{\partial y^*}\frac{\partial y^*}{\partial x} + \frac{\partial f}{\partial a^*}\frac{\partial a^*}{\partial x}\right]$$

$$= \frac{du_\tau}{dx} f + u_\tau \left[\frac{\partial f}{\partial y^*}\frac{y}{\nu}\frac{du_\tau}{dx} + \frac{\partial f}{\partial a^*}\frac{a}{\nu}\frac{du_\tau}{dx}\right] = \frac{du_\tau}{dx}\left[\frac{\partial (y^* f)}{\partial y^*} + \frac{a^*\partial f}{\partial a^*}\right]$$

The data of Willmarth et al.[18] show that the term $\partial f/\partial a^*$ is almost zero, as has been verified analytically in the solution obtained for the law of the wall, which is presented in a subsequent section. Therefore the above expression for $\partial u/\partial x$ can be approximated by

$$\frac{\partial u}{\partial x} = \frac{du_\tau}{dx}\,\frac{\partial (y^* f)}{\partial y^*} \tag{10}$$

$$\frac{\partial u}{\partial y} = \frac{u_\tau^2}{\nu}\,\frac{\partial f}{\partial y^*} \tag{11}$$

From Eqs. (2) and (10), one obtains

$$v = -\frac{\nu}{r u_\tau}\int_0^{y^*} r\,\frac{du_\tau}{dx}\,\frac{\partial (y^* f)}{\partial y^*}\,dy^*$$

or, integrating by parts,

$$v = -\frac{\nu}{u_\tau}\frac{du_\tau}{dx}\left[y^* f - \frac{1}{a^* + y^*}\int_0^{y^*} y^* f\, dy^*\right] \tag{12}$$

Then Eqs. (9), (10), (11) and (12) give

$$u\frac{\partial u}{\partial x} + v\frac{\partial u}{\partial y} = u_\tau\frac{du_\tau}{dx}\left[f(f + y^* f') - ff'y^* + \frac{f'}{a^* + y^*}\int_0^{y^*} y^* f\, dy^*\right]$$

$$= u_\tau\frac{du_\tau}{dx}\left[f^2 + \frac{f'}{a^* + y^*}\int_0^{y^*} y^* f\, dy^*\right] \tag{13}$$

where $f' = \dfrac{\partial f}{\partial y^*}$

also, with $\tau = \tau_w\tau^+ = \rho u_\tau^2\tau^+$, the right-hand side of Eq. (1) becomes

$$\frac{1}{\rho r}\frac{\partial}{\partial y}(r\tau) = \frac{u_\tau^3/\nu}{a^* + y^*}\frac{\partial}{\partial y^*}[(a^* + y^*)\tau^+] \tag{14}$$

Substitution of Eq. (13) and (14) into the boundary-layer Eq. (1) now gives

$$\frac{\partial}{\partial y^*}[(a^* + y^*)\tau^+] = -\sigma'\left[(a^* + y^*)f^2 + f'\int_0^{y^*} y^* f\, dy^*\right] \tag{15}$$

where $\sigma' \equiv \dfrac{d\sigma}{dR_x}$ $\qquad \sigma = \dfrac{U_e}{u_\tau}$, $\qquad R_x = \dfrac{U_e x}{\nu}$

Integration of Eq. (15) by parts with respect to y^* gives

$$(a^* + y^*)\tau^+\Big|_0^{y^*} = -\sigma' \left[\int_0^{y^*} (a^* + y^*) f^2 dy^* + \int_0^{y^*} f' \int_0^{y^*} y^* f\, dy^* dy^*\right]$$

$$= -\sigma' \left[a^* \int_0^{y^*} f^2 dy^* + \int_0^{y^*} y^* f^2 dy^* + f\Big|_0^{y^*} \int_0^{y^*} y^* f dy^* - \int_0^{y^*} y^* f^2 dy^*\right]$$

Since, at $y^* = 0$, $\tau^+ = 1$ and $f(0,a^*) = 0$, the above equation yields

$$\tau^+ = \frac{a^*}{a^* + y^*} \left\{1 - \sigma' \int_0^{y^*} f(\xi) \left[f(\xi) + \frac{f(y^*)}{a^*}\, \xi\right] d\xi\right\} \tag{16}$$

For small values of y^* and σ', such that the integrals in Eq. (16) are negligible, τ^+ can be approximated by

$$\tau^+ = \frac{a^*}{a^* + y^*} \tag{17}$$

On the other hand, if the inertia terms in Eq. (1) are neglected and the remaining equation is integrated with respect to y, the same expression for τ^+, given in Eq. (17), is obtained. Thus the integral term in Eq. (16),

$$c(y^*,a^*,\sigma') \equiv \sigma' \int_0^{y^*} f(\xi) \left[f(\xi) + \frac{f(y^*)}{a^*}\, \xi\right] d\xi \tag{18}$$

represents the effect of inertia on the distribution of the shear stress τ^+ across the boundary layer at a given section. The shear-stress

distribution given by Eq. (17) has been used widely in the literature. It assumes that the inertia terms in the boundary-layer equation are negligible, and hence that the stress moment, $r\tau$, is constant in the law-of-the-wall region, at a given section. The relative magnitude of the 'inertia' term in Eq. (16) can be analyzed as follows. In the blending zone, $f(y^*)$ is less than y^*, but of order $0(y^*)$. Then

$$\int_0^{y^*} f^2\, dy^* \approx 0\left(\frac{y^{*3}}{3}\right) \quad , \qquad \int_0^{y^*} y^*\, f\, dy^* \approx 0\left(\frac{y^{*3}}{3}\right)$$

Therefore, from Eq. (16),

$$\tau^+ = \frac{a^*}{a^* + y^*} - 0\left(\sigma' \frac{2}{3} y^{*3}\right) \tag{19}$$

This result can be obtained directly, without using similarity assumptions, from the Taylor-series expansion of the stress moment, $r\tau$, about $y = 0$,

$$r\tau = a\tau_w + \frac{y^2}{2} \left.\frac{\partial^2(r\tau)}{\partial y^2}\right|_{y=0} + \frac{y^3}{6} \left.\frac{\partial^3(r\tau)}{\partial y^3}\right|_{y=0} + \ldots \tag{20}$$

since $\left.\dfrac{\partial(r\tau)}{\partial y}\right|_{y=0} = 0$, as is seen from the nonslip condition and Eq. (1). Differentiation of Eq. (1) with respect to y gives

$$u_y u_x + u u_{xy} + v_y u_y + v u_{yy} = \frac{1}{\rho r} \frac{\partial^2}{\partial y^2}(r\tau) - \frac{1}{\rho r^2} \frac{\partial(r\tau)}{\partial y} \tag{21}$$

where each subscript in the above equation corresponds to either a first-order or second-order partial differentiation with respect to the subscript letter used. From the nonslip condition at $y = 0$, $u = v = u_x = 0$, from Eq. (2) at $y = 0$, we have $v_y = 0$. Therefore,

$$\left.\frac{\partial^2(r\tau)}{\partial y^2}\right|_{y=0} = 0 \tag{22}$$

Differentiation of Eq. (21), again, with respect to y, with the nonslip condition at $y = 0$, and Eq. (20), gives

$$2u_y u_{xy} + u_y v_{yy} = \frac{1}{\rho a}\left.\frac{\partial^3(r\tau)}{\partial y^3}\right|_{y=0} \tag{23}$$

Differentiation of Eq. (2) with respect to y and setting $y = 0$ gives

$$\left(u_{xy} + v_{yy}\right)_{y=0} = 0 \tag{24}$$

Also

$$\left.u_y\right|_{y=0} = \frac{\tau_w}{\mu} \quad , \qquad \left.u_{xy}\right|_{y=0} = \frac{1}{\mu}\frac{d\tau_w}{dx} = -\left.v_{yy}\right|_{y=0} \tag{25}$$

Therefore, from Eqs. (23), (24) and (25),

$$\left.\frac{\partial^3(r\tau)}{\partial y^3}\right|_{y=0} = \frac{\rho a}{\mu^2}\tau_w\frac{d\tau_w}{dx} \tag{26}$$

Substituting Eqs. (22) and (26) into (20) now gives the Taylor-series expansion of the stress as

$$\tau = \frac{a}{a + y}\ \tau_w \left(1 + \frac{\rho}{6\mu^2} \frac{d\tau_w}{dx} y^3 + \ldots\right) \tag{27}$$

or, in nondimensional form,

$$\tau^+ = \frac{a^*}{a^* + y^*} \left(1 - \frac{1}{3} \sigma'\ y^{*3} + \ldots\right) \tag{28}$$

which is in agreement with Eq. (19).

A typical value for σ' for a flat-plate boundary layer, from Ref.[12] is $\sigma' = 6 \times 10^{-6}$. Therefore, at $y^* = 30$, $\frac{\sigma'}{3} y^{*3} = 0.054$, and hence, the error in using Eq. (17) for the shear stress distribution would be order of 5.4%. As y^* increases, the contribution from the inertia term $c(y^*, a^*, \sigma')$ would increase. Consequently, the error would be larger in using Eq. (17) for the shear-stress distribution rather than Eq. (16).

1.3 Numerical Solution of the Law of the Wall

Under the assumption of similarity, Eq. (6), together with Eqs. (8) and (16), defines the law of the wall for the axisymmetric turbulent boundary layer. From Eqs. (6) and (8),

$$\frac{\partial f}{\partial y^*} = \frac{2\tau^+}{1 + [1 + 4\kappa^2 y^{*2} \tanh(\lambda^2 y^{*2})\tau^+]^{\frac{1}{2}}} \tag{29}$$

$$\tau^+ = \frac{a^*}{a^* + y^*} \left\{1 - \sigma' \int_0^{y^*} f(\xi) \left[f(\xi) + \frac{f(y^*)}{a^*}\ \xi\right] d\xi\right\} \tag{16}$$

For various values of a^* and σ', this pair of equations has been solved simultaneously by using the modified Adams-Bashforth method and Simpson's 1/3 rule, respectively. The distribution of the shear stress given by Eqs. (16) and (17) is shown in Fig. 2. The law-of-the-wall range increases as a^* increases. For the largest value of y^*, where the law of the wall is valid, estimated from Willmarth's data, the contributions of the inertia terms to the shear-stress distribution for $\sigma' = 10^{-5}$ and for the various values of a^* is shown in Table 1.1.

TABLE 1.1 ERROR DUE TO INERTIA TERMS

a^*	y^*	$\tau_o^+ = a^*/(a^* + y^*)$	$\tau^+ = \tau_o^+(1 - c)$	correction to τ^+ (%)
50	169	0.2283	0.2265	0.794
100	244	0.2907	0.2872	1.203
500	444	0.5297	0.5196	1.893
1000	544	0.6477	0.6333	2.217

Also, knowing that $c(y^*, a^*, \sigma')$ is much less than 1, and writing Eq. (16) in the form $\tau^+ = \tau_o^+(1 - c)$, then from Eq. (6), one obtains

$$u^* \simeq \int_0^{y^*} \frac{2\tau_o^+(1 - c/2)dy^*}{1 + \sqrt{1 + 4\ell^{*2}\tau_0^+}} \quad , \qquad \tau_o^+ = \frac{a^*}{a^* + y^*}$$

This shows that, the percentage error introduced by using τ_o^+, rather than $\tau^+ = \tau_o^+(1 - c)$, is reduced by a factor of two in the nondimensional

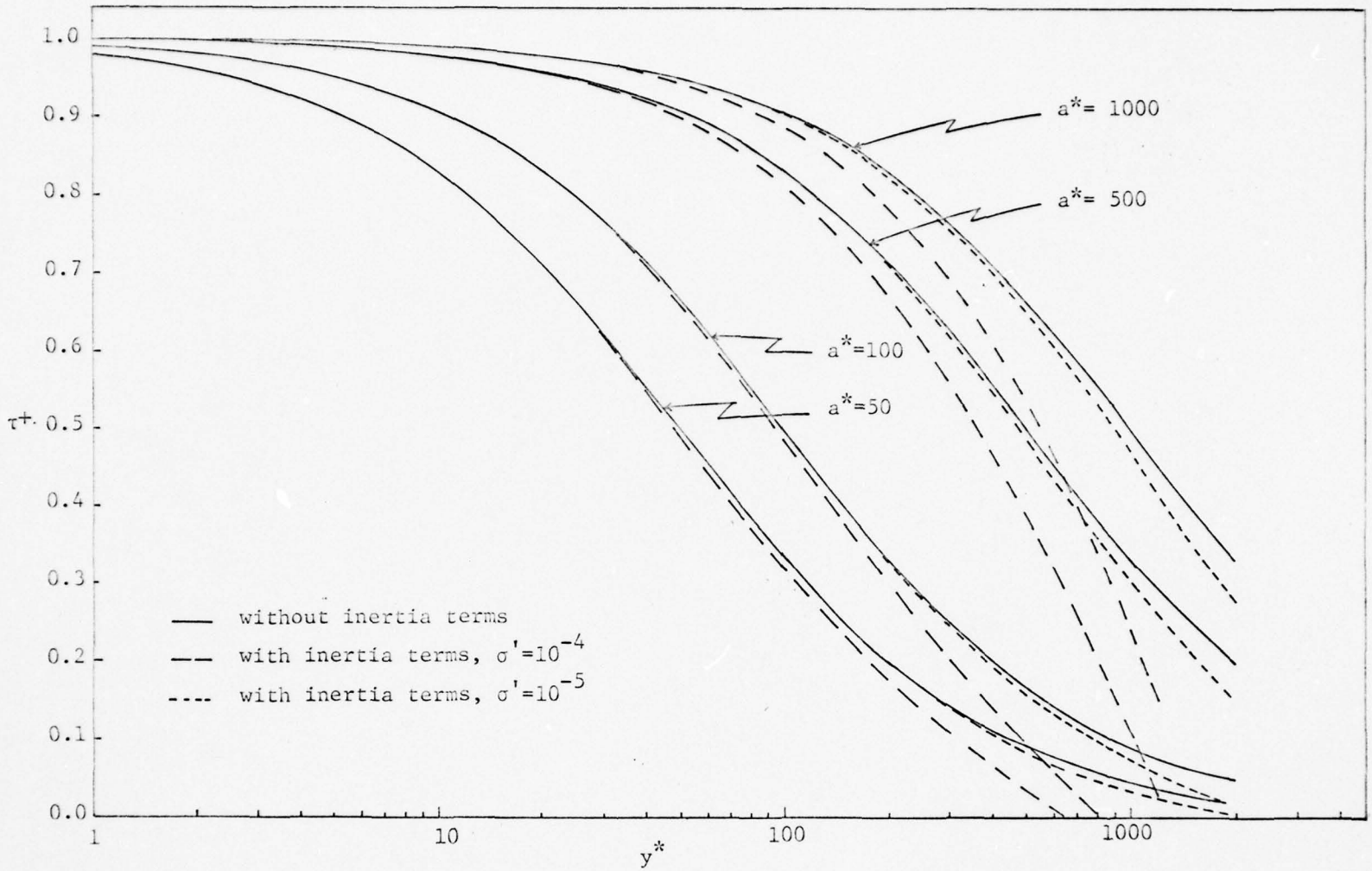

Figure 2. Distribution of Shear Stress in Law-of-the-Wall Region

velocity distribution, u^*. Therefore the effect of the inertia terms on the shear stress and, consequently, on the velocity distributions can be neglected if $\sigma' \leq 10^{-5}$, which is consistent with the assumed functional form, $u^* = f(y^*, a^*)$. However, if the inertia terms are not negligible, the functional form for u^* should be $f(y^*, a^*, \sigma')$, where $\sigma' = \sigma'(R_x, a^*)$. Therefore, throughout the remainder of this study, the inertia terms will be neglected in the law-of-the-wall region. Hence the distribution of the shear stress may be approximated by Eq. (17).

1.4 Analysis of Distribution of the Mixing Length

Generally, the flow in the so-called inner layer is subdivided into three regions, namely: a) viscous sublayer, b) blending zone, and c) fully turbulent zone. In the viscous sublayer, the Reynolds stresses are generally assumed to be negligible compared to viscous stresses; hence the mixing length is $\ell^* = 0$. With $\ell^* = 0$ and $\tau^+ = \dfrac{a^*}{a^* + y^*}$, Eq. (6) gives the sublayer relation as

$$u^* = a^* \ln(1 + y^*/a^*) \tag{30}$$

For a flat-plate boundary layer, the viscous sublayer relation is:

$$u^* = y^*, \qquad y^* < 5 \tag{31}$$

Therefore, Eq. (30) represents a generalization of the linear relation for axisymmetric boundary layers. For the fully turbulent region, the viscous stresses are generally neglected in comparison with the Reynolds stresses, and the mixing length is taken as $\ell^* = \kappa y^*$.

For thin boundary layers, there are various mixing-length models. The mixing-length model, $\ell^* = \kappa y^* \sqrt{\tanh(\lambda^2 y^{*2})}$, given by Landweber and Poreh[12], and discussed by Patel[11], gives the correct asymptotic behavior and is continuous throughout the law-of-the-wall range. However, in the case of a thick axisymmetric turbulent boundary layer developing on a cylinder of constant radius, it is more likely that there is a direct influence of the transverse curvature on the turbulence, and hence on the mixing length, so that it may not be realistic to adopt mixing-length models established for thin boundary layers, as has been done in the literature. Indeed, the experimental results presented by Patel, Nakayama and Damian [20], for the thick boundary layer near the tail of a body of revolution showed that mixing length is directly influenced by transverse curvature, and that the mixing length decreases markedly as the boundary-layer thickness increases relative to the local radius of curvature.

The mixing length is generally interpreted as the average distance over which eddies transport momentum without losing their identity. Also, it is known that the large eddies contribute more to momentum transfer than small eddies. Hence the mixing length, ℓ, may be taken to be proportional to the size of the large eddies, particularly to the dimension perpendicular to the direction of the main flow. Due to the geometry, the circumference about the circular cylinder increases linearly with the distance from the wall. Thus, in the inner layer, eddies on a circular cylinder can stretch more transversely, and hence are shorter in the dimension perpendicular to the direction of the main

flow compared to the eddies of equivalent volume on a flat plate. Consequently, it is reasonable to expect the mixing length to be reduced for turbulent boundary layers growing on circular cylinders. In other words, since the region influenced by the shear force on circular cylinders increases as the distance from the wall, the intensity of shear force will be decreased compared to the flat wall, and hence the eddy size and consequently the mixing length will be reduced. The experimental results of Singh and Afzal[19], also confirm that eddy sizes about a circular cylinder are smaller than those of a flat plate.

For a thin boundary layer, the sublayer relation is: $u^* = y^*$, and the mixing length in the fully turbulent region is: $\ell^* = \kappa y^*$. For an axisymmetric turbulent boundary layer, the sublayer relation is: $u^* = a^* \ln(1 + y^*/a^*)$. Hence, this suggests, by direct analogy, that in the fully turbulent region, the mixing length should be replaced by

$$\ell^* = \kappa a^* \ln(1 + y^*/a^*) \tag{32}$$

This analogy is reasonable, because:

i) For a thick boundary layer, Eq. (32) yields smaller values of the mixing length than for a thin boundary layer, as required.

ii) It has the correct asymptotic behavior, since

$$\lim_{a^* \to \infty} a^* \ln(1 + y^*/a^*) = \lim_{a^* \to \infty} a^* \left\{ \frac{y^*}{a^*} - \frac{1}{2}\left(\frac{y^*}{a^*}\right)^2 \right\} = y^*$$

and hence $\lim_{a^* \to \infty} \kappa a^* \ln(1 + y^*/a^*) = \kappa y^*$

$$\text{iii)} \quad \lim_{a^* \to 0} a^* \ln\left(1 + \frac{y^*}{a^*}\right) = \lim_{a^* \to \infty} \ln \frac{(1 + a^* y^*)}{a^*} = \lim_{a^* \to \infty} \frac{1}{1 + a^* y^*} = 0$$

This is consistent with the relaminarization process observed in axisymmetric turbulent boundary layers. Consequently, for the axisymmetric turbulent boundary layer, Eq. (8) will be assumed to be given by

$$\ell^* = \kappa a^* \ln(1 + y^*/a^*) \sqrt{\tanh(\lambda^2 y^{*2})} \tag{33}$$

1.5 Analytical Solution in the Fully Turbulent Region

Once the distribution of the shear stress and the mixing length are established, the velocity distribution can be obtained from Eq. (6) by using a proper numerical integration scheme. Substitution of Eqs. (17) and (33) into Eq. (6) gives the velocity distribution as

$$u^* = \int_0^{y^*} \frac{2a^* dy^*}{(a^* + y^*)\left\{1 + \left[1 + 4\kappa^2 a^{*2} \ln^2(1 + y^*/a^*) \tanh(\lambda^2 y^{*2}) \frac{a^*}{a^* + y^*}\right]^{1/2}\right\}} \tag{34}$$

In the fully turbulent region, from order-of-magnitude considerations, Eq. (34) can be simplified and integrated analytically. In the fully turbulent region, $\tanh(\lambda^2 y^{*2})$ approaches unity and the term $4\kappa^2 a^{*2} \ln^2(1 + y^*/a^*) \frac{a^*}{a^* + y^*}$ is much greater than one. Hence Eq. (34) reduces to

$$u^* = \int_{y_o^*}^{y^*} \frac{\sqrt{a^*}\, dy^*}{\sqrt{a^* + y^*}\ \kappa a^* \ln(1 + y^*/a^*)} + B_r(a^*) \tag{35}$$

where $B_r(a^*)$ is the integral of Eq. (34) from zero to y^*, the value of y^* at which flow becomes fully turbulent. The change of variables, $z^2 = 1 + y^*/a^*$, transforms Eq. (35) to the well-known Logarithmic integral [21]

$$u^* = \frac{1}{\kappa} \int_{z_o}^{z} \frac{dz}{\ell n z} + B_r(a^*) \tag{36}$$

Since $z = \sqrt{1 + y^*/a^*} > 1$, Eq. (36) may be expressed as the well-known Exponential integral [21],

$$u^* = \frac{1}{\kappa} \left(E_i[\ell n\sqrt{1 + y^*/a^*}] - E_i[\ell n\sqrt{1 + y_o^*/a^*}] \right) + B_r(a^*)$$

or, alternatively, as

$$u^* = \frac{1}{\kappa} E_i[\ell n\sqrt{1 + y^*/a^*}] + B'(a^*) \tag{37}$$

where $B'(a^*) = \frac{-1}{\kappa} E_i[\ell n\sqrt{1 + y_o^*/a^*}] + B_r(a^*)$

Also $E_i(x)$ is given in terms of the infinite series

$$E_i(x) = \gamma + \ell n x + \sum_{n=1}^{\infty} \frac{x^n}{n \cdot n!} \tag{38}$$

where $\gamma = 0.5772156 \cdots$ is the Euler constant. Therefore, in terms of the infinite series, the velocity distribution in the fully turbulent region is given by

$$u^* = \frac{1}{\kappa} \ln \left[\ln\sqrt{1 + y^*/a^*}\right] + \frac{1}{\kappa} \sum_{n=1}^{\infty} \frac{[\ln(1 + y^*/a^*)]^n}{2^n \, n \cdot n!} + B'(a^*) + \gamma \tag{39}$$

When $a^* \to \infty$, $\qquad u^* \approx \frac{1}{\kappa} \ln y^* + B$ (40)

Comparison with the asymptotic form of Eq. (39) then yields

$$B'(a^*) + \gamma = \frac{1}{\kappa} \ln 2a^* + B(a^*) \tag{41}$$

and hence Eq. (38) becomes

$$u^* = \frac{1}{\kappa} \ln \left[a^* \ln \left(1 + \frac{y^*}{a^*}\right)\right] + \frac{1}{\kappa} \sum_{n=1}^{\infty} \frac{[\ln(1 + y^*/a^*)]^n}{2^n \, n \cdot n!} + B(a^*) \tag{42}$$

It is interesting to note that, in 1967, from purely heuristic considerations, Rao [6] proposed that the logarithmic law for the axisymmetric boundary layers should be given by

$$u^* = \frac{1}{\kappa} \ln \left[a^* \ln \left(1 + \frac{y^*}{a^*}\right)\right] + B \tag{43}$$

where B is the usual constant for the flat-plate boundary layer. Rao obtained this expression simply by replacing y^* in Eq. (40) by the sublayer relation $a^* \ln \left(1 + \frac{y^*}{a^*}\right)$.

The infinite series in Eq. (42) converges very rapidly. For $y^*/a^* \leq 2$, five terms and for $y^*/a^* \leq 5$, seven terms are sufficient to calculate u^* to five significant figures. For $y^*/a^* = 5$, and $a^* = 100$, the first term of the series is 20% of $\ln[a^* \ln(1 + y^*/a^*)]$, but as a^*

increases and y^*/a^* decreases, the contribution from the infinite series decreases. The following table shows the contribution of the infinite series for some typical values of y^* taken from Willmarth's data [18].

TABLE 1.2 COMPARISON OF RELATIVE MAGNITUDES OF TERMS IN EQ. (42)

a^*	y^*	y^*/a^*	1†	2‡	3††	4§
198.2	227.4	1.147	5.020	0.3820	0.4219	0.73%
198.2	323.5	1.632	5.2565	0.4839	0.5493	1.13%
271.4	326.3	1.2023	5.3672	0.3948	0.4374	0.73%
1376	1981	1.4393	7.1123	0.4459	0.5009	0.72%

† $\ell n[a^* \ell n(1 + y^*/a^*)]$

‡ $\frac{1}{2} \ell n(1 + y^*/a^*)$ (first term of series)

†† $\sum_{n=1}^{5} \frac{[\ell n(1 + y^*/a^*]^n}{2^n \, n \cdot n!}$

§ % error due to neglecting the infinite series after the first term.

Equation (34) has been integrated for various values of λ and compared with Willmarth's data [18]. The results show that λ is constant and equal to $\sqrt{3}/63$. With this value of λ, Eq. (34) gives the complete velocity distribution in the law-of-the-wall region. Hence, using the results from Eq. (34), the value of $B(a^*)$ can be calculated directly from Eq. (42). The variation of $B(a^*)$ with respect to $1/a^*$ is linear, as shown in Fig. 3, and can be written as

$$B(a^*) = -\frac{41.758}{a^*} + 5.45 \tag{44}$$

Also, as shown in Table 1.2, the largest contribution of the infinite series comes from the first term. Neglecting the rest of the infinite series, Eq. (42) can be written as

$$u^* = \frac{1}{\kappa} \ell n \left[a^* \sqrt{1 + \frac{y^*}{a^*}}\, \ell n \left(1 + \frac{y^*}{a^*}\right)\right] - \frac{41.758}{a^*} + 5.45 \tag{45}$$

For $y^*/a^* < 1$, the argument of the logarithm can be expanded as

$$Y^* \equiv a^* \sqrt{1 + \frac{y^*}{a^*}}\, \ell n \left(1 + \frac{y^*}{a^*}\right) \approx a^* \left[1 + \frac{1}{2}\left(\frac{y^*}{a^*}\right) - \frac{1}{8}\left(\frac{y^*}{a^*}\right)^2 + \cdots\right]$$

$$\times \left[\frac{y^*}{a^*} - \frac{1}{2}\left(\frac{y^*}{a^*}\right)^2 + \frac{1}{3}\left(\frac{y^*}{a^*}\right)^3 - \cdots\right]$$

$$= y^* \left[1 - \frac{1}{24}\left(\frac{y^*}{a^*}\right)^2 + \frac{1}{24}\left(\frac{y^*}{a^*}\right)^3 + \cdots\right] \tag{46}$$

Therefore the argument of the logarithm, Y^*, behaves very nearly like y^*, even in the neighborhood of $y^*/a^* = 1$. Also

$$\frac{\partial u^*}{\partial a^*} = \frac{\partial f(y^*, a^*)}{\partial a^*} \approx \frac{41.758}{a^{*2}}$$

These results verify the assertion in Sec. 1.2 that $\partial f/\partial a^*$ is negligible.

The data of Willmarth et al [18] are compared with Eq. (34) and with the solution of Patel [11] in Fig. 4-Fig. 8. A comparison of Eq. (34) and Eq. (45) is also given in Fig. 4. As can be seen from this figure, the analytical approximation of Eq. (34), i.e. Eq. (45), is in excellent agreement in the range of the logarithmic portion of the law of the wall, even for the smallest value of a^*. Also, Fig. 9 compares the data of Willmarth et al [18] with Eq. (45) for various values of a^* and δ/a. It is important to emphasize that the argument Y^* given by Eq. (46) behaves very nearly like y^* in the neighborhood of $y^*/a^* = 1$. This explains why the Preston-tube technique with the usual calibration curve gives good measurements of the wall shear stress, and why some of the previous researchers, like Yu [8] and Chin et al. [9], whose data are limited to $\delta/a < 2$, were able to keep the form of the classical two-dimensional logarithmic law.

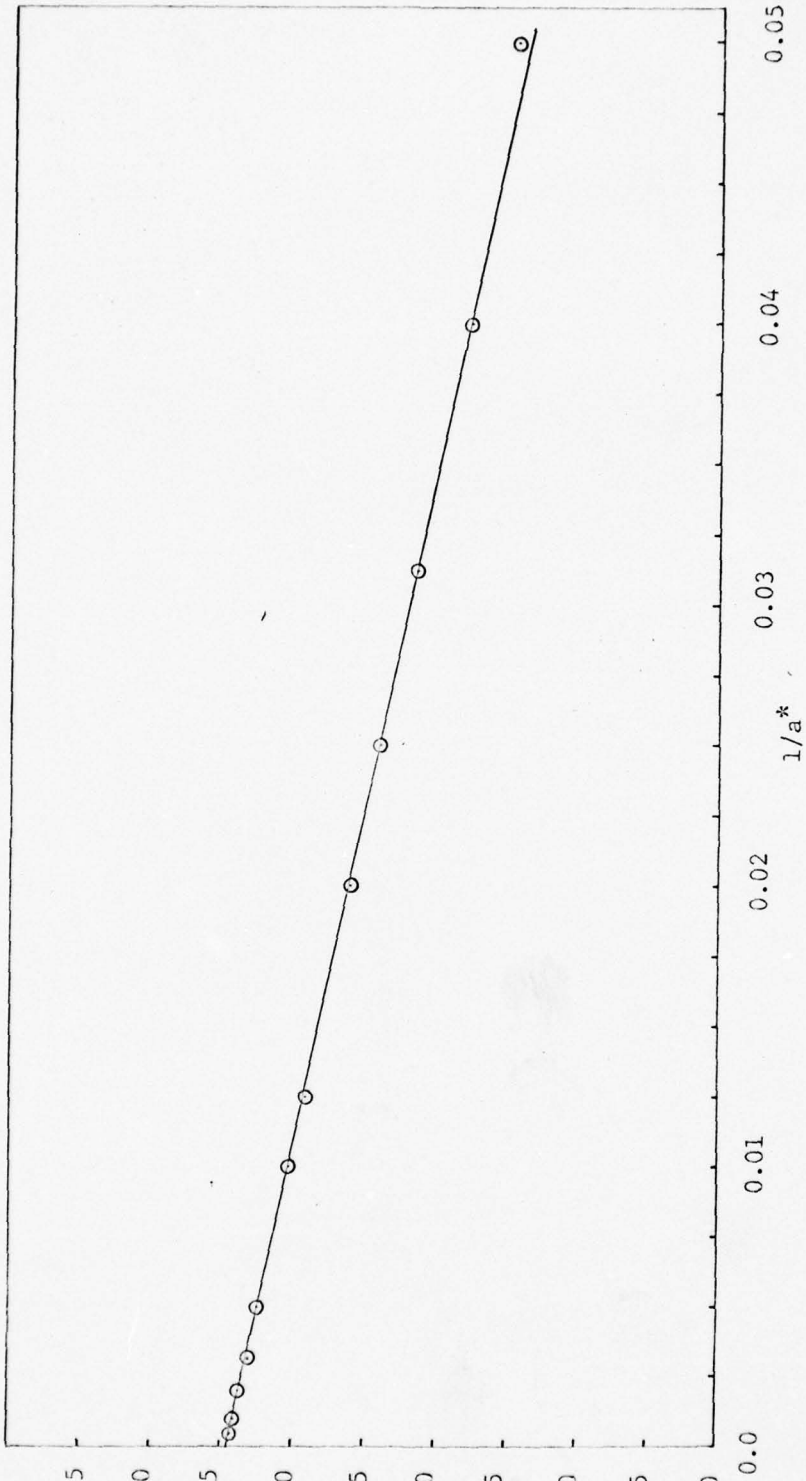

Figure 3. Computed Variation of B(a*) with 1/a*

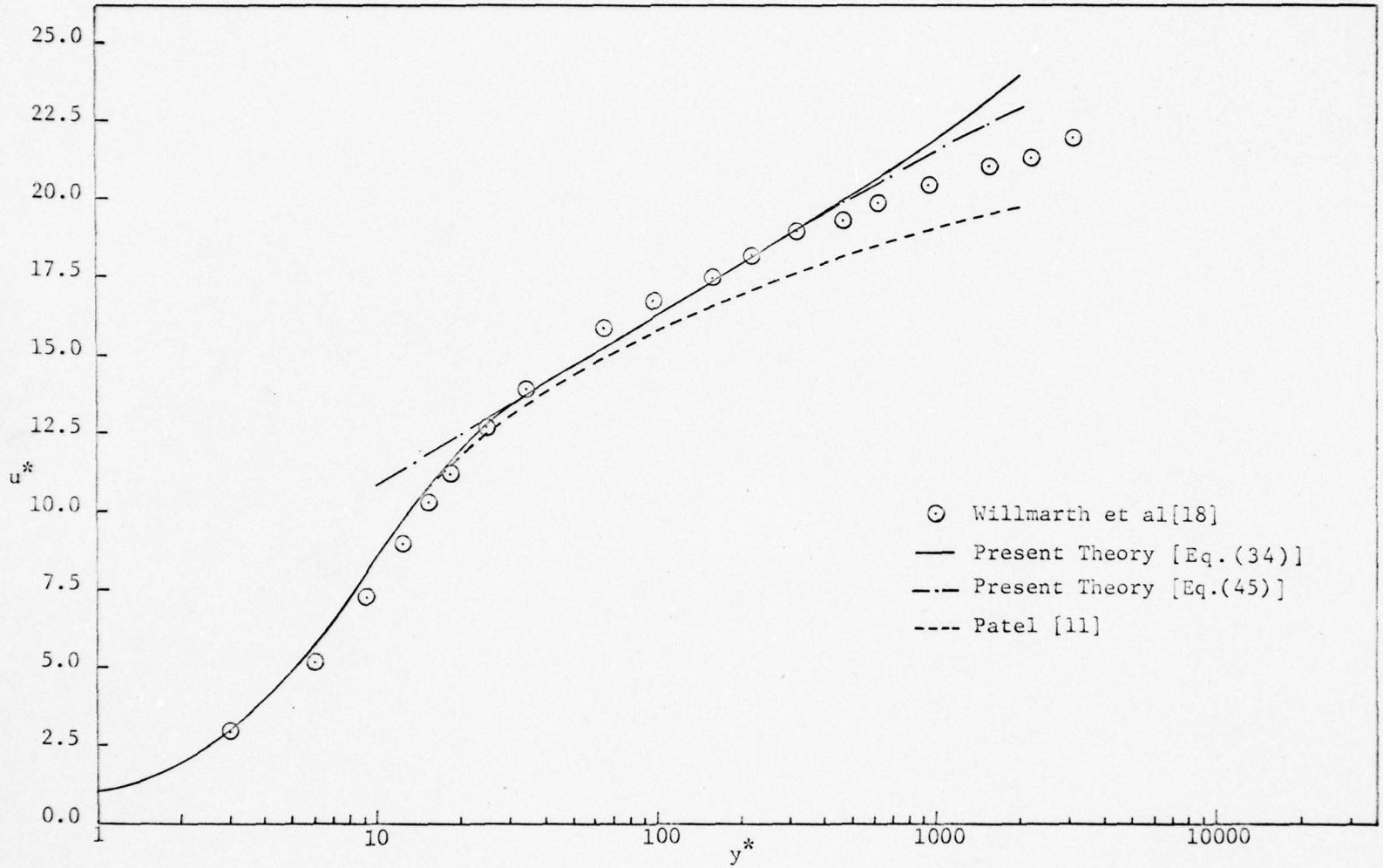

Figure 4. Law of the Wall for $\delta/a = 16$, $a^* = 198.2$

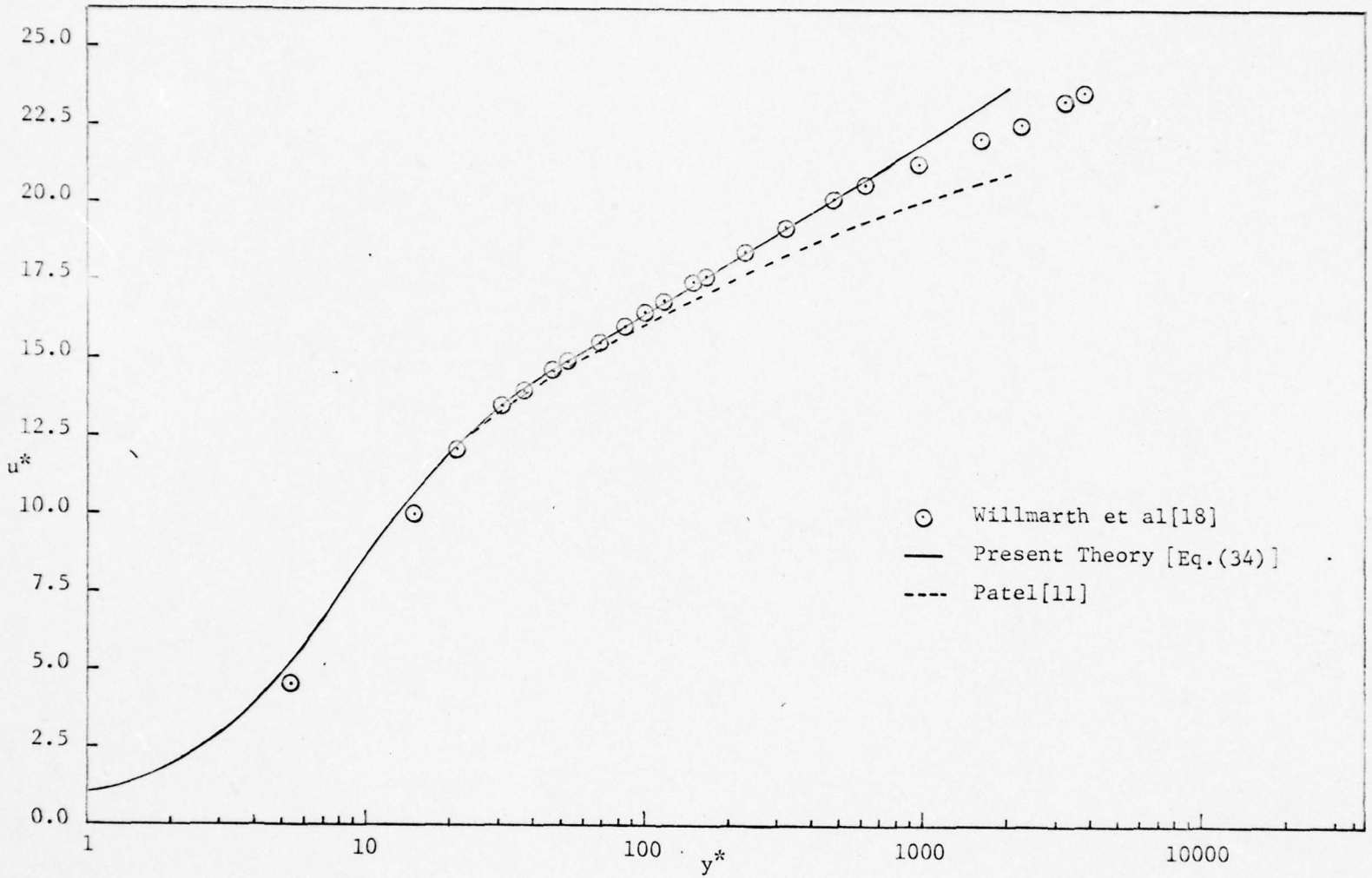

Figure 5. Law of the Wall for $\delta/a = 9.45$, $a^* = 398.2$

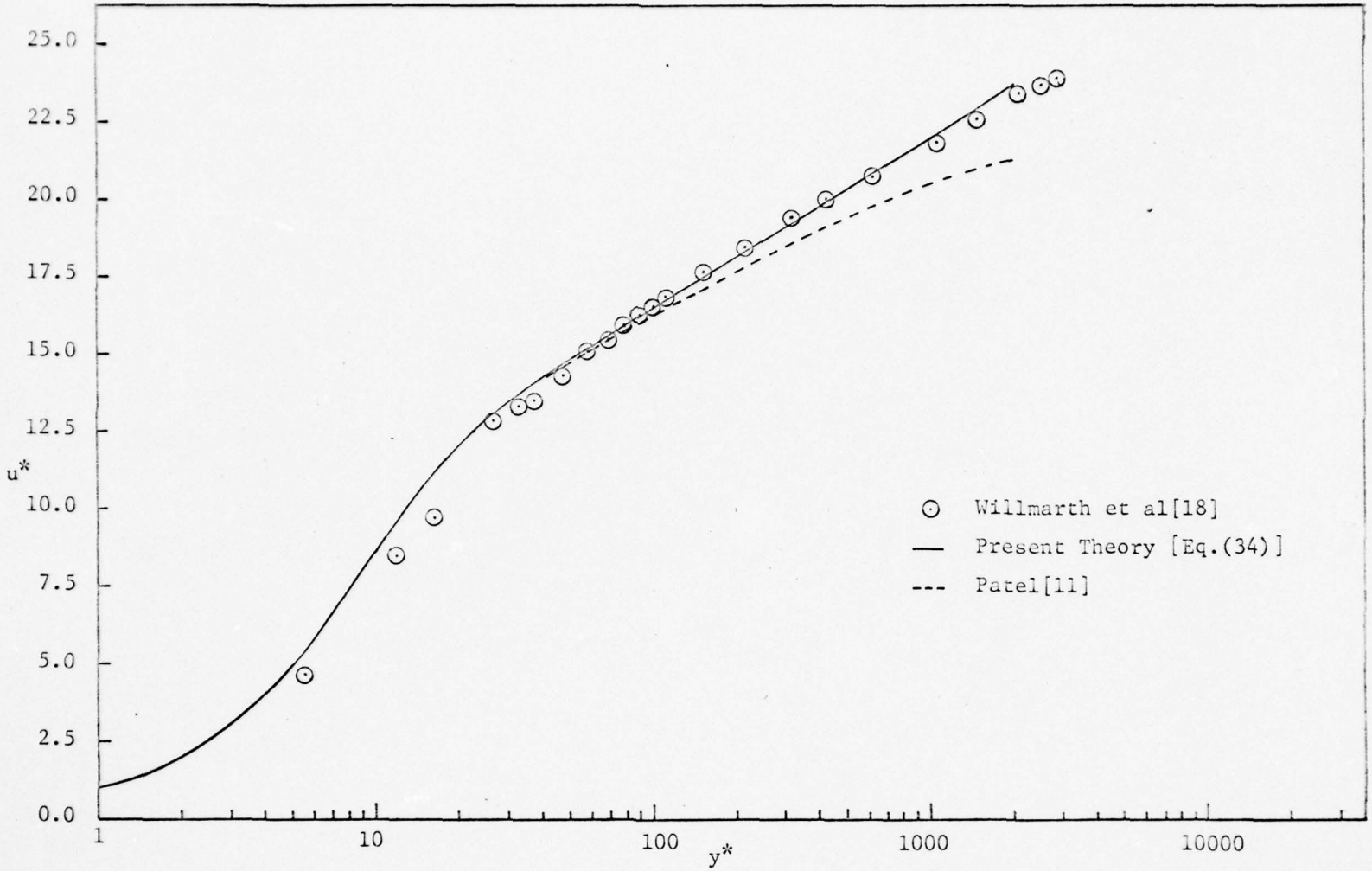

Figure 6. Law of the Wall for $\delta/a = 5.52$, $a^* = 531$

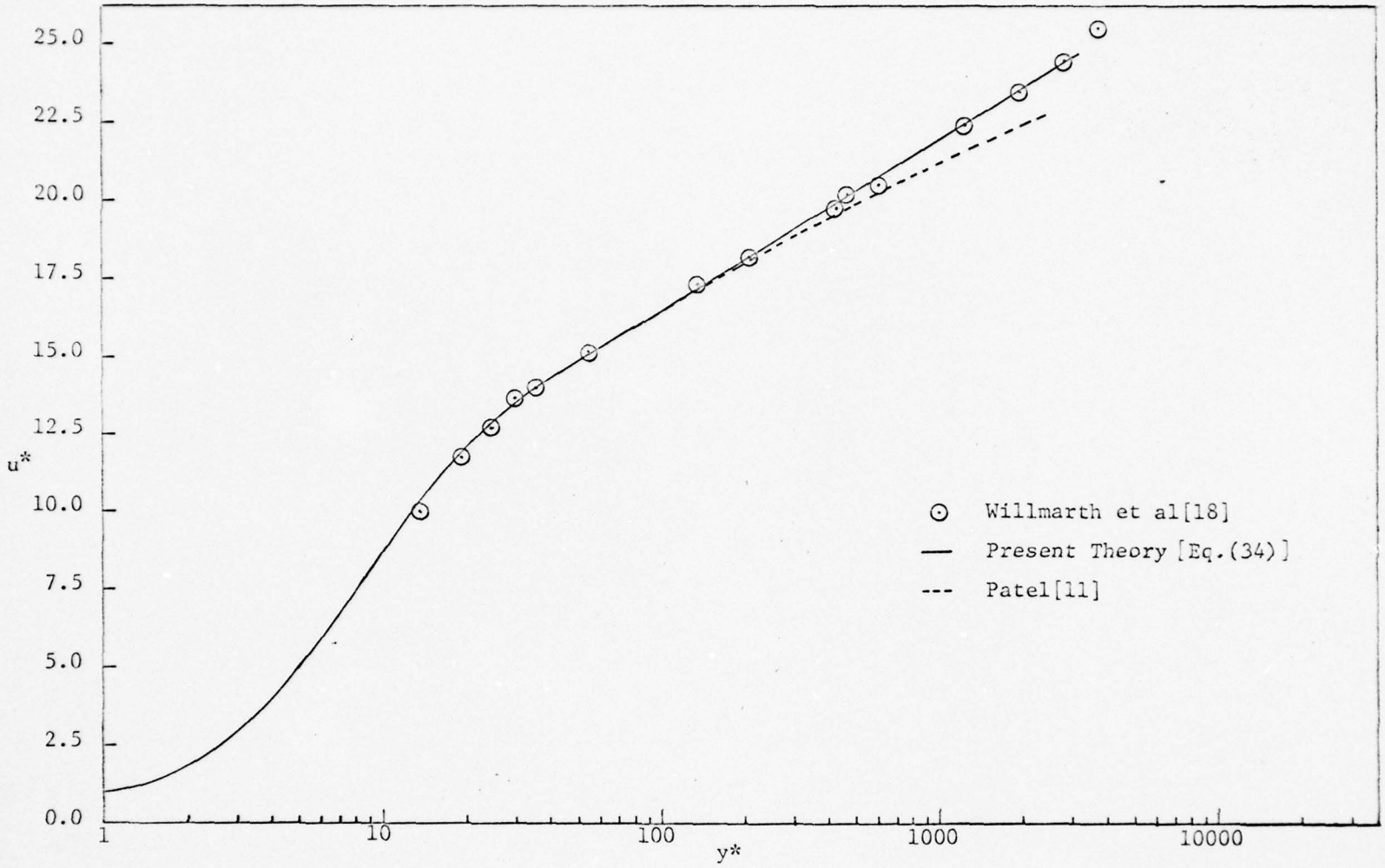

Figure 7. Law of the Wall for $\delta/a = 4.12$, $a^* = 1376$

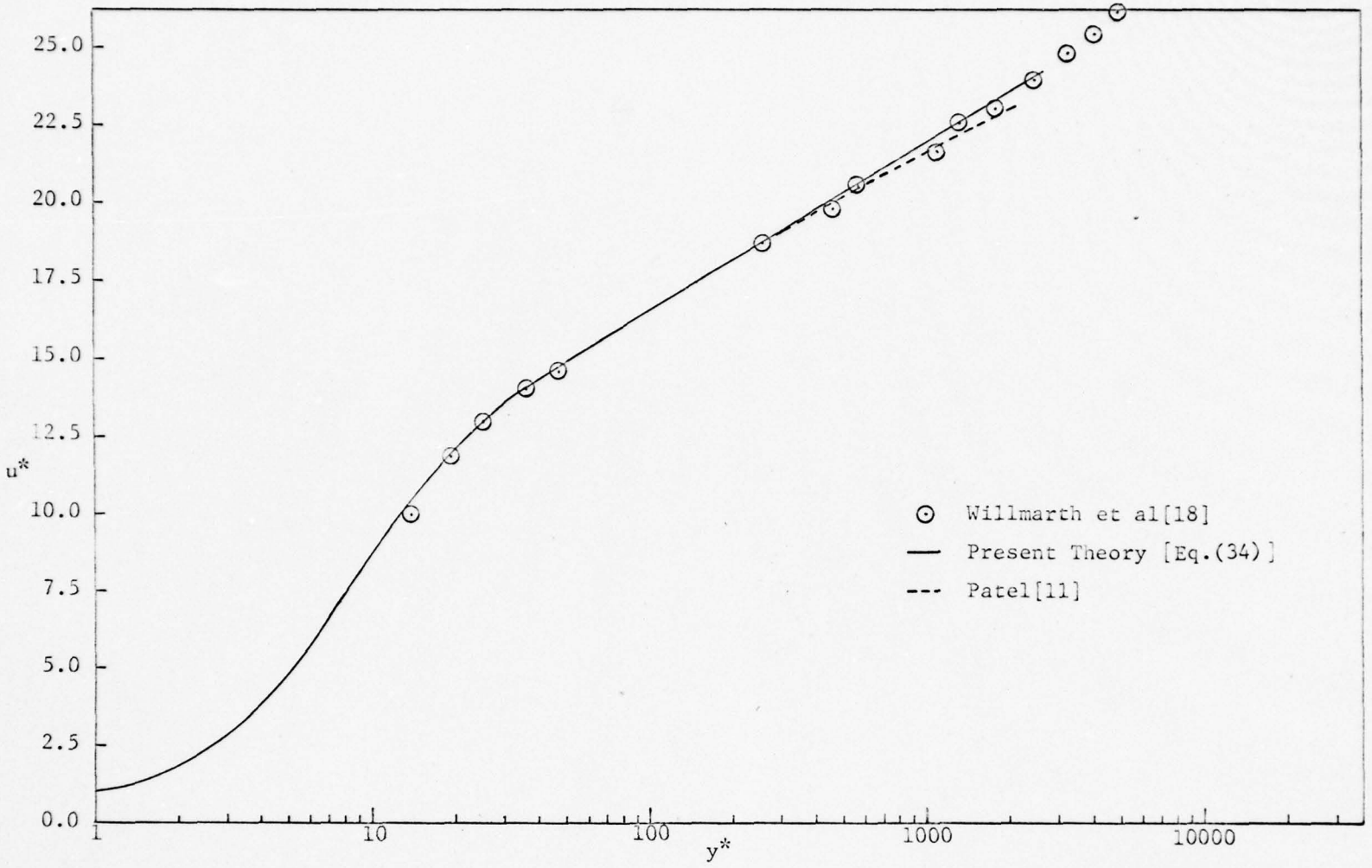

Figure 8. Law of the Wall for $\delta/a = 1.76$, $a^* = 2833$

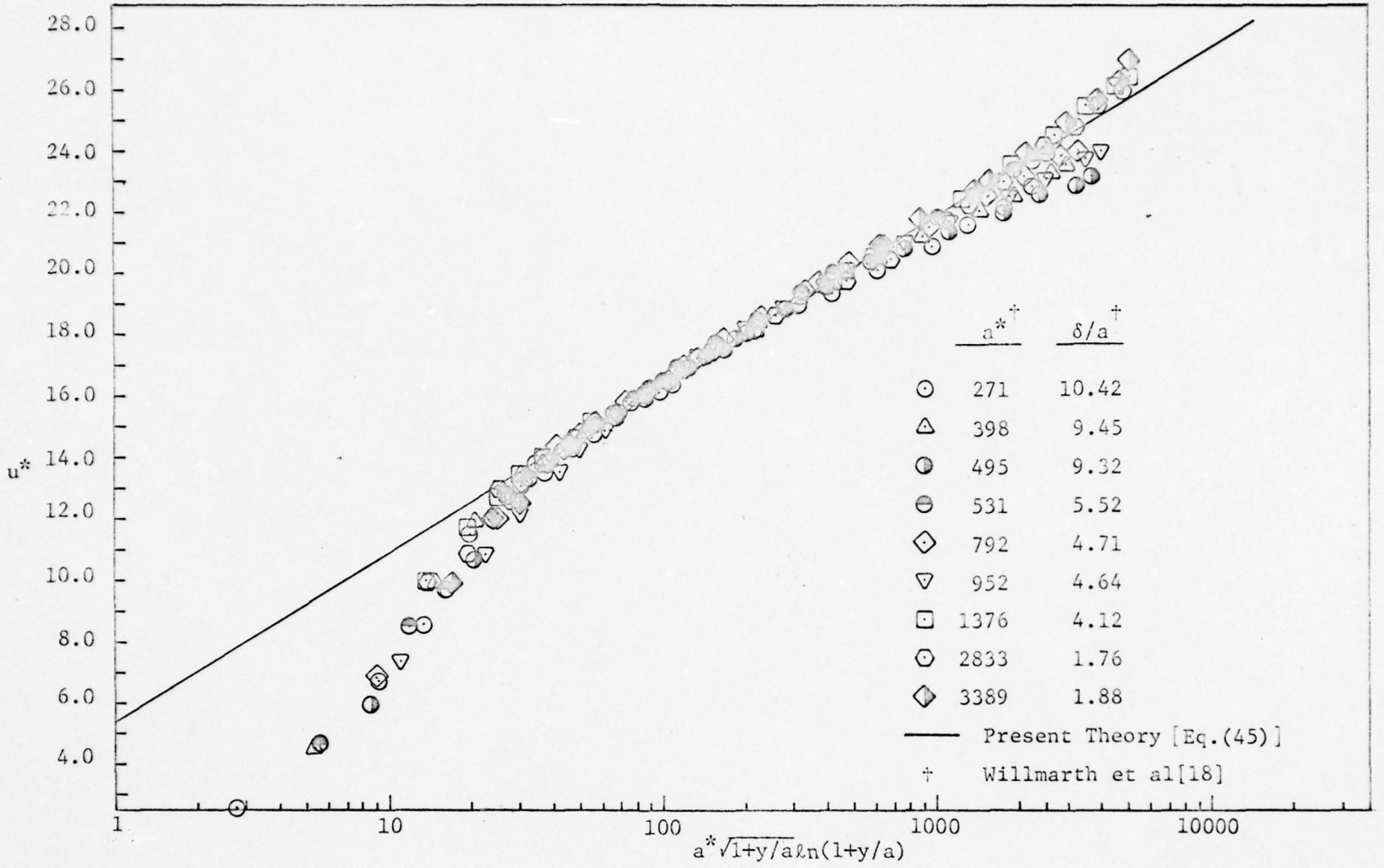

Figure 9. Logarithmic Portion of Law of the Wall

CHAPTER 2

THE VELOCITY-DEFECT LAW

2.1 General Approach

Unrestricted rotational flows which are of finite lateral extent and carried along by the mean velocity of the external free stream are defined as wake flows. The retarded flow downstream of a solid body placed in a free stream of uniform velocity is governed by a constant total force applied to the fluid by the solid body. It is this constant drag force that determines the motion in the wake, when self-preserving flow has been attained. Except for the inner boundary condition, the equations of the mean flow u and the boundary conditions for an axisymmetric wake are exactly the same as the mean-flow equations of a boundary layer growing on a cylinder of a constant radius, given by Eqs. (1), (2), (3) and (4) in the previous chapter. A thick, axisymmetric boundary layer is attained on an infinitely long cylinder when the radius of the cylinder is very small relative to the distance x from the nose. If the boundary-layer thickness relative to the transverse radius of curvature is large, the cylinder may be considered as a small vorticity- and turbulence-producing disturbance. Consequently, the flow might be considered similar to a wake flow with the modified inner boundary condition. The important difference is that the drag generating the wake is a function of the longitudinal coordinate in the present problem. With these considerations, the

velocity-defect law has been derived in a manner similiar to that which has been used for the axisymmetric turbulent wake under the following assumptions:

i) As stated in the previous chapter, the curvatures of the mean-flow streamlines are negligible; hence $v << u$.

ii) The velocity gradient, $\partial u/\partial r$, is small in the region of the velocity-defect law.

iii) Oseen's approximation is valid.

Under these assumptions, the mean-flow equation takes the following form:

$$U_e \frac{\partial u_d}{\partial x} = - \frac{1}{\rho r} \frac{\partial}{\partial r} (r\tau) \tag{47}$$

where $u_d = U_e - u$ satisfies the boundary condition

$$\lim_{r \to \infty} u_d(x,r) = 0 \tag{48}$$

The solution for the laminar boundary layer for the thick axisymmetric flow along a circular cylinder of constant radius, given by Glauert and Lighthill [3], suggests that the proper axial length scale for correlating a thick boundary layer is $\xi^2 = \frac{x}{aRe_a}$, where Re_a is the Reynolds number based on cylinder radius a, and the free-stream velocity U_e. On the other hand, the solutions for laminar and turbulent wakes give the same mathematical form for the velocity profile if the eddy-viscosity concept is used. Therefore, for the present problem, the use of the following nondimensional quantities seems to be appropriate:

$$\xi^2 = \frac{x}{aRe_a} \quad , \qquad \bar{u}_d = \frac{u_d \sqrt{Re_a}}{U_e} \quad , \qquad R = \frac{\delta + a}{a}$$

$$\tau^+ = \frac{\tau}{\rho u_\tau^2} \quad , \qquad \bar{r} = \frac{r}{a} \tag{49}$$

With these nondimensional quantities, Eq. (47) becomes

$$\frac{\beta^2}{\xi} \frac{\partial \bar{u}_d}{\partial \xi} = -\frac{1}{\bar{r}} \frac{\partial}{\partial \bar{r}} (\bar{r} \tau^+) \tag{50}$$

where

$$\beta^2 \equiv \frac{\sigma^2}{2\ Re_a^{3/2}} \quad , \qquad \sigma = \frac{U_e}{u_\tau} \tag{51}$$

If the velocity variation across the boundary layer in the velocity-defect zone is small compared with the free-stream velocity, then the flow may be self-preserving. This suggests that the nondimensional velocity defect $\bar{u}_d$ may then be of the separable form

$$\bar{u}_d = \chi(\xi)\ f(\eta) \tag{52}$$

where

$$\eta = \frac{r}{\delta + a} = \frac{\bar{r}}{R} \tag{53}$$

The boundary condition at $\eta = 1$ is

$$\bar{u}_d = 0 \quad , \qquad \tau^+ = 0 \tag{54}$$

Then one obtains

$$\frac{\partial \bar{u}_d}{\partial \xi} = \dot{\chi} f(\eta) + \chi \frac{df}{d\eta} \frac{d\eta}{dR} \frac{dR}{d\xi} = \dot{\chi} f(\eta) - \frac{\chi \dot{R}}{R} \eta f' \tag{55}$$

where

$$\dot{\chi}(\xi) = \frac{d\chi}{d\xi} \quad , \qquad \dot{R} = \frac{dR}{d\xi} \quad , \qquad f' = \frac{df}{d\eta} \tag{56}$$

and substitution of Eqs. (52) and (55) into Eq. (50) gives

$$\frac{\beta^2 R}{\xi} \left(\dot{\chi} f - \frac{\chi \dot{R}}{R} \eta f' \right) = - \frac{1}{\eta} \frac{\partial}{\partial \eta} (\eta \tau^+) \tag{57}$$

Integrating Eq. (57) with respect to η from η to 1, and using boundary conditions given by Eq. (54) yields, after some manipulation,

$$\frac{\beta^2 \dot{R} \chi}{\xi} \left\{ \eta^2 f + \left(2 + \frac{R \dot{\chi}}{\dot{R} \chi} \right) \int_\eta^1 \eta f \, d\eta \right\} = \eta \tau^+ \tag{58}$$

Equation (58) is the basic equation for the velocity-defect law. In order to solve it, the variation of the shear stress needs to be modeled. Depending on the modeling of the shear stress, Eq. (58) gives different differential equations for $\chi(\xi)$ and $f(\eta)$, as will be shown later.

2.2 Eddy-Viscosity Approach

The numerical solution of Cebeci [14] showed that transverse curvature does not affect eddy viscosity directly. Cebeci used the free-stream velocity and the two-dimensional displacement thickness as the characteristic velocity and the length scale, respectively, in his

treatment. In general, for free turbulent flows such as jets and wakes, eddy viscosity, as a function of the longitudinal coordinate, gives very good results. Since it has been stated that the flow in the velocity-defect region might be considered as a wake flow, the eddy viscosity may be assumed to be a function of the longitudinal coordinate, ξ, only. Hence, the distribution of the shear stress in terms of eddy viscosity, $\varepsilon(\xi)$, is given by

$$\tau = \rho\varepsilon \frac{\partial u}{\partial r} = -\rho\varepsilon \frac{\partial \bar{u}_d}{\partial r} \tag{59}$$

Substitution of the nondimensional quantities given by Eq. (49) and the velocity defect given by Eqs. (52) and (53) into Eq. (59) gives

$$\rho u_\tau^2 \tau^+ = -\rho\varepsilon \frac{U_e}{\sqrt{Re_a}} \frac{\partial \bar{u}_d}{\partial \eta} \frac{\partial \eta}{\partial r} = -\rho\varepsilon \frac{U_e}{\sqrt{Re_a}} \frac{\chi}{aR} \varepsilon' \tag{60}$$

or

$$\tau^+ = -\varepsilon \frac{U_e}{u_\tau^2 \sqrt{Re_a}} \frac{\chi}{aR} f' = -\frac{2\varepsilon}{\nu} \beta^2 \frac{\chi}{R} f' \tag{61}$$

Substituting Eq. (61) into Eq. (58) and rearranging gives

$$-\frac{1}{\eta f'} \left\{ \eta^2 f + \left(2 + \frac{R\dot{\chi}}{\dot{R}\chi} \right) \int_\eta^1 \eta f \, d\eta \right\} = 2 \frac{\varepsilon(\xi)}{\nu} \frac{\xi}{\dot{R}R} \tag{62}$$

The similarity assumption requires that

$$2 + \frac{R\dot{\chi}}{\dot{R}\chi} = 2b \quad , \qquad \text{a constant} \tag{63}$$

and

$$2\,\frac{\varepsilon(\xi)}{\nu}\,\frac{\xi}{R\dot{R}} = \alpha^2 \quad , \qquad \text{a constant} \tag{64}$$

The solution of Eq. (63), obtained by the method of separation of variables, is

$$\chi(\xi) = CR^{2(b-1)} \tag{65}$$

where C is a constant of integration.

In order to solve Eq. (64), it is necessary to know the function $\varepsilon(\xi)$. For an axisymmetric turbulent wake, ε/ν is proportional to the longitudinal coordinate x with a power law as $x^{-1/3}$. Since, it has been suggested that the flow in the velocity-defect region is analogous to axisymmetric wake flow, ε/ν may be assumed to be

$$\frac{\varepsilon(\xi)}{\nu} = \lambda\xi^{m-1} \tag{66}$$

where m and λ are constants. Hence, after substituting Eq. (66), Eq. (64) gives the differential equation for the boundary-layer thickness R as

$$R\dot{R} = \frac{2\lambda}{\alpha^2}\,\xi^m \tag{67}$$

Integration of Eq. (67) gives

$$R^2 + K = \frac{4\lambda}{\alpha^2}\,\frac{\xi^{m+1}}{m+1} = A^2\,\xi^{m+1} \quad , \qquad A = \frac{2}{\alpha}\sqrt{\frac{\lambda}{m+1}} \tag{68}$$

where K is a constant of integration. From Eq. (68), we obtain

$$R = A\,\xi^{\frac{m+1}{2}}\left(1 + \frac{K}{R^2}\right)^{-1/2} \tag{69}$$

After substituting $\xi^2 = \frac{x/a}{Re_a}$, Eq. (69) takes the form

$$R = A\left(\frac{x/a}{Re_a}\right)^{\frac{m+1}{4}}\left[1 + \frac{K}{R^2}\right]^{-1/2} \tag{70}$$

Equation (65) then becomes

$$\chi(\xi) = C\left[A\left(\frac{x}{a\ Re_a}\right)^{\frac{m+1}{4}}\left(1 + \frac{K}{R^2}\right)^{-1/2}\right]^{2(b-1)} \tag{71}$$

or

$$\chi = B\left(\frac{x/a}{Re_a}\right)^{\frac{m+1}{2}(b-1)}\left(1 + \frac{K}{R^2}\right)^{(1-b)} \tag{72}$$

where $B = CA^{2(b-1)}$.

From Eq. (62), the equation for $f(\eta)$ is

$$\eta^2 f + 2b\int_{\eta}^{1} \eta f\, d\eta + \alpha^2\,\eta f' = 0 \tag{73}$$

Differentiation of Eq. (73) with respect to η gives

$$\alpha^2\,\eta f'' + (\alpha^2 + \eta^2)f' + 2(1 - b)\,\eta f = 0 \tag{74}$$

The change of variables $\eta = \alpha\zeta$ eliminates α^2 in Eq. (74), which then reduces to

$$\zeta f'' + (1 + \zeta^2) f' + 2(1 - b)\zeta f = 0 \tag{75}$$

This satisfies the boundary condition

$$\lim_{\zeta \to \infty} f(\zeta) = 0 \tag{76}$$

2.3 Solution of the Differential Equation for f(η)

The assumptions of similarity and the eddy-viscosity model have led to the second-order linear differential equation

$$f''(\zeta) + \left(\zeta + \frac{1}{\zeta}\right) f'(\zeta) + 2(1 - b) f(\zeta) = 0 \tag{77}$$

where $\zeta = \eta/\alpha$, and α and b are parameters to be evaluated from the boundary condition and the experimental data. This differential equation has two singular points, at $\zeta = 0$ and $\zeta = \infty$. Since, $\zeta(\zeta + \frac{1}{\zeta}) = \zeta^2 + 1$ is analytic and regular everywhere, $\zeta = 0$ is a regular singular point. Therefore, Eq. (77) has at least one nontrivial solution of the form

$$f(\zeta) = \zeta^s \sum_{k=0}^{\infty} a_k \zeta^k \tag{78}$$

In order to determine the behavior of Eq. (77) at infinity, put $t = 1/\zeta$; then the behavior of Eq. (77) at infinity can be obtained as t goes to zero. With the transformation $t = 1/\zeta$, Eq. (77) then becomes

$$\frac{d^2f}{dt^2} + \left(\frac{1}{t} - \frac{1}{t^3}\right) \frac{df}{dt} + 2(1 - b) \frac{1}{t^4} f = 0 \tag{79}$$

which is not regular at $t = 0$. Since $t\left(\frac{1}{t} - \frac{1}{t^3}\right) = 1 - \frac{1}{t^2}$. Therefore, $t = 0$ and hence $\zeta = \infty$ is an irregular singular point. Hence, a non-trivial regular solution may or may not exist in the neighborhood of $\zeta = \infty$.

On the other hand, the exact solutions of Eq. (77) can easily be obtained for the values of $b = 0, 1/2, 1$.

Case 1: $b = 0$

$$f'' + \left(\zeta + \frac{1}{\zeta}\right) f' + 2f = 0 \tag{80}$$

which can be put into the form

$$\frac{d}{d\zeta} [\zeta f' + \zeta^2 f] = 0 \tag{81}$$

Integration of Eq. (81) once gives

$$\zeta f' + \zeta^2 f = C_1 \tag{82}$$

The solution of this first-order linear differential equation is

$$f(\zeta) = e^{-\zeta^2/2} \left(C_1 \int \frac{e^{\zeta^2/2}}{\zeta} \, d\zeta + C_2\right) \tag{83}$$

This solution with $C_1 = 0$ corresponds to the wake-flow solution.

Case 2: $b = 1/2$

$$f'' + \left(\zeta + \frac{1}{\zeta}\right) f' = 0 \tag{84}$$

The solution of Eq. (84) is

$$f(\zeta) = e^{-\zeta^2/4} \left(C_1 I_o\left(\frac{\zeta^2}{4}\right) + C_2 K_o\left(\frac{\zeta^2}{4}\right)\right) \tag{85}$$

where $I_o(\frac{\zeta^2}{4})$ and $K_o(\frac{\zeta^2}{4})$ are the Bessel function of the first kind and the modified Bessel function of the second kind, of order zero, respectively.

Case 3: $b = 1$

$$f'' + \left(\zeta + \frac{1}{\zeta}\right) f' = 0 \tag{86}$$

Separation of variables gives the solution as

$$f(\zeta) = C_1 \int \frac{e^{-\zeta^2/2}}{\zeta} d\zeta + C_2 \tag{87}$$

or, in series form,

$$f(\zeta) = \frac{C_1}{2} \left\{ \ell n \frac{\zeta^2}{2} - \frac{\zeta^2}{2} + \frac{\zeta^4}{2 \cdot 2!} - \frac{\zeta^6}{3 \cdot 3!} + \cdots \right\} + C_2 \tag{88}$$

This case is impossible, according to Eq. (65), since the velocity defect $\bar{u}_d$ decreases and $R(\xi)$ increases with increasing values of ξ; i.e. b must be less than 1.

The exact solutions of the differential equation for b = 0, 1/2, 1 suggest the form of $f(\zeta)$ to be

$$f(\zeta) = e^{-z} F(z) \quad , \qquad z = \zeta^2/2 \tag{89}$$

Substitution of the transformation given by Eq. (89) into Eq. (77) reduces the latter equation to

$$zF''(z) + (1 - z) F'(z) - bF(z) = 0 \tag{90}$$

Equation (90) is a confluent hypergeometric differential equation, particularly known as the Kummer differential equation. It has a regular singularity at z = 0, and an irregular singularity at $z = \infty$. The method of Fröbenius gives only one linearly independent solution. In order to give a general solution of the differential equation, it is necessary to find another linearly independent solution. The two linearly independent solutions are given by Abramowitz and Stegun [21] as

$$F_1(z) = {}_1F_1(b,1,z) = M(b,1,z)$$

$$F_2(z) = U(b,1,z) = -\frac{1}{\Gamma(b)} \left\{ {}_1F_1(b,1,z) \ln z + \sum_{n=0}^{\infty} \frac{(b)_n z^n}{(n!)^2} [\psi(b+n) - 2\psi(1+n)] \right\} \tag{91}$$

where

$$(b)_n = b(b+1)(b+2) \cdots (b+n-1) \quad , \qquad (b)_o = 1 \tag{92}$$

$\psi(b + n)$ is the logarithmic derivative of the gamma function, which is known as the Digamma (psi) function, and given as

$$\psi(b+n) = \frac{1}{(n-1)+b} + \frac{1}{(n-2)+b} + \cdots + \frac{1}{2+b} + \frac{1}{1+b} + \frac{1}{b} + \psi(b) \quad (93)$$

where $\psi(b) = \frac{d}{db}[\ell n\, \Gamma(b)]$ is tabulated in Abramowitz and Stegun [21].

${}_1F_1(b,1,z)$ is the confluent hypergeometric function, particularly known as the Kummer function. The other notations for Kummer functions are $M(b,1,z)$ and $\phi(b,1,z)$. In series form, ${}_1F_1(b,1,z)$ is given by

$${}_1F_1(b,1,z) = \sum_{n=0}^{\infty} \frac{(b)_n}{(n!)^2} z^n = \frac{1}{\Gamma(b)} \sum_{n=0}^{\infty} \frac{\Gamma(b+n)}{(n!)^2} z^n \quad (94)$$

In the neighborhood of $z = \infty$, the solutions $F_1(z) = M(b,1,z)$ and $F_2(z) = U(b,1,z)$ have simple asymptotic expansions given by

$$F_1(z) = M(b,1,z) \approx z^{b-1} e^z \sum_{n=0}^{\infty} \frac{(1-b)_n (1-b)_n}{n!} z^{-n} \quad (95)$$

$$F_2(z) = U(b,1,z) \approx z^{-b} \sum_{n=0}^{\infty} \frac{(b)_n (b)_n}{n!} (-z)^{-n} \quad (96)$$

For $z \to \infty$

$$F_1(z) = M(b,1,z) \approx \frac{1}{\Gamma(b)} e^z z^{b-1} [1 + O(|z|^{-1})] \quad (97)$$

$$F_2(z) = U(b,1,z) \approx z^{-b}[1 + O(|z|^{-1})] \quad (98)$$

Therefore, the general solution for $f(\eta)$ is

$$f(\eta) = e^{-z} F(z) = e^{-z}[C_1 M(b,1,z) + C_2 U(b,1,z)] \quad (99)$$

and, as $z \to \infty$, $(\eta \to \infty)$

$$f(\eta) \approx C_1 \frac{z^{b-1}}{\Gamma(b)} + C_2\, e^{-z}\, z^{-b} + O(|z|^{-1}) \tag{100}$$

In the outer region of the boundary layer, it is assumed that the mean flow behaves like an axisymmetric wake. The solution of an axisymmetric wake with the eddy viscosity assumption gives the defect-velocity profiles in terms of an exponential function. Hence, if the boundary layer behaves as an axisymmetric wake in the velocity-defect region, the constant C_1 must be zero. Therefore, the solution for $f(\eta)$ is

$$f(\eta) = e^{-z}\, U(b,1,z) \quad , \qquad z = \frac{\eta^2}{2\alpha^2} \tag{101}$$

From Eq. (52), (65) and (101), the velocity defect is

$$\bar{u}_d = C\, R^{2(b-1)}\, e^{-z}\, U(b,1,z) \tag{102}$$

where b, C and α are the constants to be determined from the experimental data. On the other hand, the following analysis indicates the possible range of the values of b.

The nondimensional displacement thickness for an axisymmetric flow is defined as

$$\frac{\delta_1}{a} = \int_1^R \left(1 - \frac{u}{U_e}\right) \frac{r}{a}\, d\left(\frac{r}{a}\right) = \int_1^{r_c} \frac{u_d}{U_e}\, \bar{r}\, d\bar{r} + \int_{r_c}^R \frac{u_d}{U_e}\, \bar{r}\, d\bar{r} \tag{103}$$

where r_c is the point of intersection of the two laws, the law of the wall and the velocity-defect law. Since the flow area increases with

radial distance, the major contribution to displacement thickness comes from the velocity-defect region for a thick axisymmetric turbulent flow. Therefore, the nondimensional displacement thickness can roughly be approximated by

$$\frac{\delta_1}{a} \approx \int_{r_c}^{R} \frac{u_d}{U_e} \bar{r}\, d\bar{r} \tag{104}$$

Substituting Eq. (102) and $z = \dfrac{\bar{r}^2}{2R^2\alpha^2}$ into Eq. (104) gives

$$\frac{\delta_1}{a} \approx \alpha^2\, CR^{2b} \int_{z_o}^{\frac{1}{2}\alpha^2} e^{-z}\, U(b,1,z)\,dz \quad , \qquad z_o = \frac{\bar{r}_c^2}{2R^2\alpha^2} \tag{105}$$

Since the displacement thickness δ_1 increases with the boundary layer thickness δ, b must be a positive number. Thus we have $0 < b < 1$.

From Eqs. (91) and (94), the Kummer function U(b,1,z) can be written as

$$U(b,1,z) = \frac{1}{\Gamma(b)} \left\{ \sum_{n=0}^{\infty} \frac{(b)_n\, z^n}{(n!)^2} \left[\ell nz + \psi(b+n) - 2\psi(1+n) \right] \right\} \tag{106}$$

This series is convergent for all values of z. Let $N \gg 1$; then

$$U(b,1,z) = -\frac{1}{\Gamma(b)} \sum_{n=0}^{N-1} \frac{(b)_n\, z^n}{(n!)^2} \left[\ell nz + \psi(b+n) - 2\,\psi(1+n) \right] + R_N \tag{107}$$

where

$$R_N = -\frac{1}{\Gamma(b)} \sum_{n=N}^{\infty} \frac{(b)_n\, z^n}{(n!)^2} \left[\ell nz + \psi(b+n) - 2\psi(1+n) \right] \tag{108}$$

since $0 < b < 1$, $(b)_n = b(b+1)(b+2)\cdots(b+n-1) < n!$,

$n = 1,2,3,\cdots$ and when $n \to \infty$

$$\psi(b+n) \simeq \ln(b+n) - \frac{1}{2(b+n)} - \frac{1}{12(b+n)^2} + \frac{1}{120(b+n)^2} + \cdots$$

$$\psi(b+n) < \psi(1+n) \sim \ln(n+1)$$

Therefore

$$|R_N| < \frac{1}{\Gamma(b)} \sum_{n=N}^{\infty} \frac{z^n}{n!}[\ln z - \psi(1+n)] < \frac{1}{\Gamma(b)} \sum_{n=N}^{\infty} \frac{z^n}{n!}[\ln z(n+1)] \quad (109)$$

$$\frac{\ln[z(N+1)]}{N} > \frac{\ln[z(n+1)]}{n}, \qquad n > N$$

Hence

$$|R_N| < \frac{z^N \ln[z(N+1])}{\Gamma(b)(N-1)!}\left[1 + \frac{z}{N} + \frac{z^2}{N(N+1)} + \cdots\right]$$

$$< \frac{z^N \ln[z(N+1)]}{\Gamma(b)(N-1)!}\left[1 + \frac{z}{N}\,\frac{z^2}{N^2} + \frac{z^3}{N^3} + \cdots\right]$$

For $z < N$, $1 + \frac{z}{N} + \frac{z^2}{N^2} + \cdots + \cdots = \frac{1}{1 - \frac{z}{N}}$

Therefore

$$|R_N| < \frac{1}{\Gamma(b)} \frac{z^N \ln[z(N+1)]}{(N-1)!\,(1 - \frac{z}{N})} \quad (110)$$

For $z = 5$, $N = 25$, $|R_N| < \frac{2.92 \times 10^{-6}}{\Gamma(b)}$

Therefore, the series in Eq. (106) can be truncated at n = 25 for $z \leq 5$. For larger values of z, the asymptotic expansion given by Eq. (96) should be used. Also, as $|z| \to 0$, one obtains

$$U(b,1,z) = -\frac{1}{\Gamma(b)} \quad (\ell nz + \psi(b) + O(|z\ell nz|) \tag{111}$$

Equations (70) and (101) contain six undetermined constants; namely A, m, K, b, C and α. These constants have been determined from the data of Willmarth et al [18], and Keshavan [7]. In Eq. (69), as ξ goes to zero, R goes asymptotically to one. Hence the constant K must be of order unity. Consequently, for large values of R, the factor $\left(1 + \frac{K}{R^2}\right)^{-\frac{1}{2}}$ in Eq. (70) is negligible. The plot of $\xi^2 = \frac{x/a}{Re_a}$ versus $R = \frac{\delta + a}{a}$ on log-log paper, for large values of R, then gave the value of m as 7/13, from the slope of the best straight line drawn through the data, as shown in Fig. 10. Once the value of m had been obtained, the values of K and A were evaluated according to Eq. (68), by using all the available data. The values found were A = 18.5 and K = -2.

The values of b, α and C (or B) were determined solely from the data of Willmarth et al [18]. Let

$$S = S(z) = Ce^{-z}\, U(b,1,z)$$

$$Y = \bar{u}_d = \left(1 - \frac{u}{U_e}\right)\sqrt{Re_a}$$

then, according to Eq. (102),

$$Y = S(z)\, R^{2(b-1)} \tag{112}$$

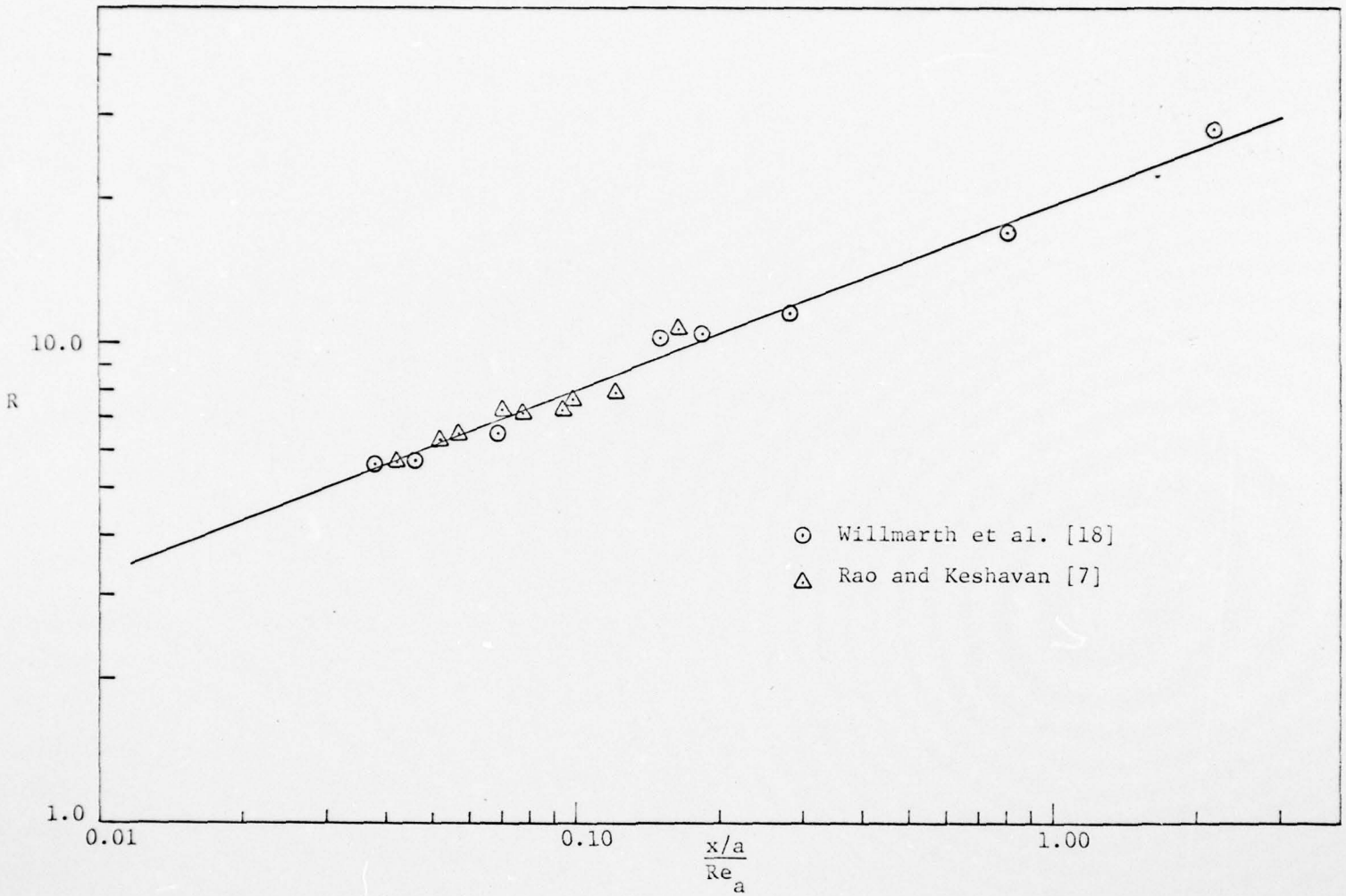

Figure 10. Determination of value of m in Eq. (70)

Therefore, for each assigned value of $z = z_i$, the graph of Y versus R on log-log paper should give a straight line of slope $2(b - 1)$ and intercept $S(z_i)$, according to Eq. (112). Willmarth's data were plotted according to Eq. (112) for various constant values of z(or η), as shown in Fig. 11. The value of b, determined from the slope, was $b = 0.35$. Therefore, from Eq. (72), $\chi(\xi)$ becomes

$$\chi = B\sqrt{\frac{a}{x}}\ \sqrt{Re_a}\ \left(1 - \frac{2}{R^2}\right)^{0.65} \tag{113}$$

Hence, from Eqs. (52) and (101), the velocity defect becomes

$$\frac{U_e - u}{U_e} = B\sqrt{\frac{a}{x}}\ \left(1 - \frac{2}{R^2}\right)^{0.65} e^{-z}\ U(b,1,z) \quad , \qquad z = \frac{\eta^2}{2\alpha^2} \tag{114}$$

Let

$$Z = \sqrt{\frac{x}{a}}\ \frac{U_e - u}{U_e}\ \left(1 - \frac{2}{R^2}\right)^{-0.65} \tag{115}$$

and

$$T = e^{-z}\ U(b,1,z) \quad , \qquad b = 0.35 \quad , \qquad z = \frac{\eta^2}{2\alpha^2} \tag{116}$$

After applying Eqs. (115) and (116), Eq. (114) becomes

$$Z = BT \tag{117}$$

The values of Z were obtained from Willmarth's data. The values of T, corresponding to the same values of η, were calculated from Eq. (116)

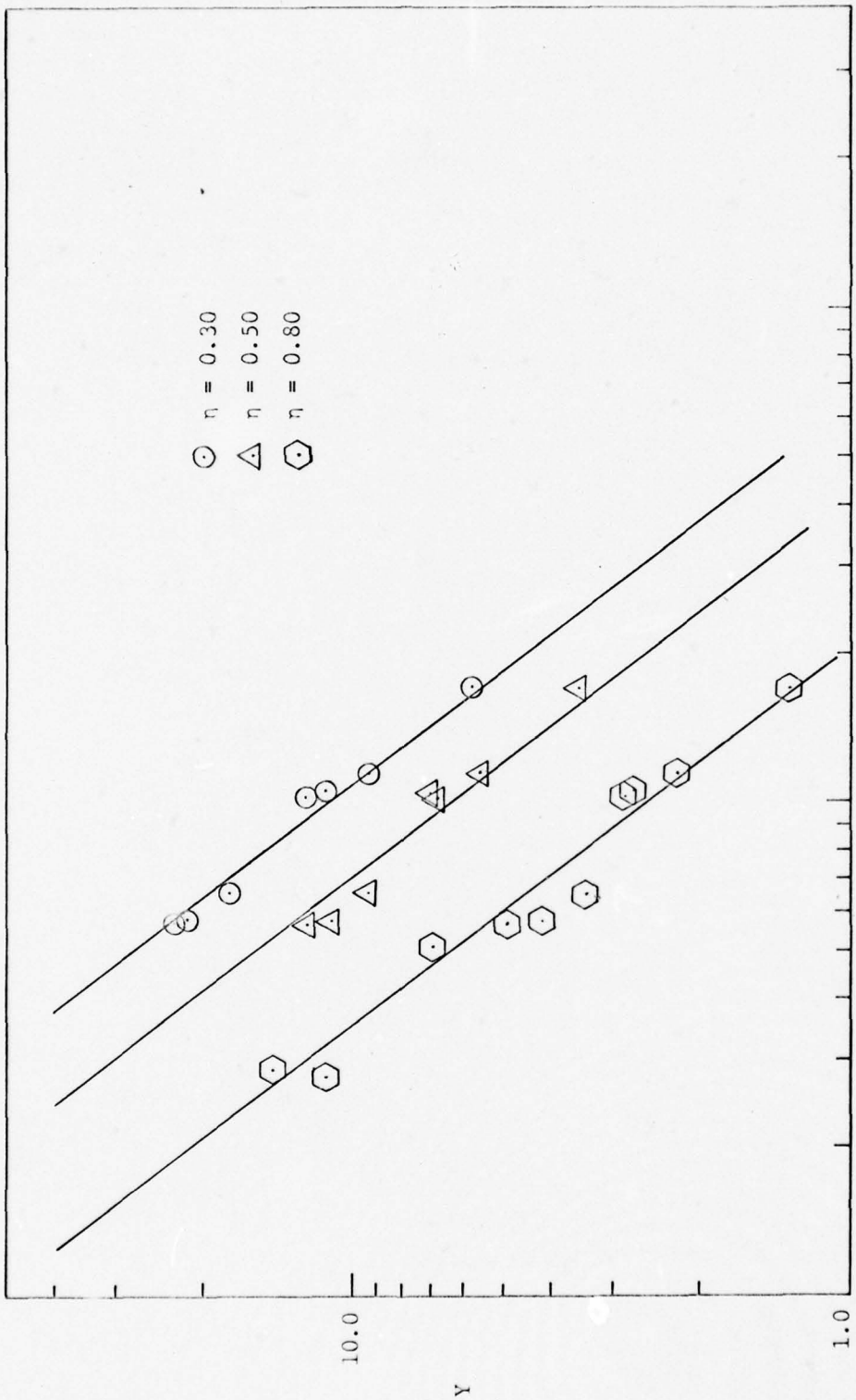

Figure 11. Determination of value of b.

for a range of values of α. The value of α which gave the best straight line passing through the origin was chosen. Consequently, the slope of the best straight line gave the value of B. The results are as follows:

$$R\sqrt{1-\frac{2}{R^2}} = 18.5\left(\frac{x/a}{Re_a}\right)^{5/13} \tag{118}$$

$$\frac{U_e - u}{U_e} = 4\sqrt{\frac{a}{x}}\left(1-\frac{2}{R^2}\right)^{0.65} e^{-z}\, U(b,1,z) \quad , \qquad z = \frac{\eta^2}{2\alpha^2} \tag{119}$$

$$\alpha = 1/2 \quad , \qquad b = 0.35$$

Comparisons with the data of Willmarth et al. [18], and Keshavan [7] are shown in Figs. 12 and 13.

2.4 The Mixing - Length Approach

The mixing length for the outer part of the boundary layer and the wake is generally assumed to be constant and proportional to a characteristic length at a given section. For this problem, the mixing length ℓ, in the velocity-defect region will be assumed to be given by

$$\bar{\ell} = \frac{\ell}{a} = \lambda_\ell R \quad , \qquad R = \frac{\delta + a}{a} \tag{120}$$

where λ_ℓ is a constant to be determined from the available data. Then the shear-stress distribution is given by

$$\tau = \rho \ell^2 \left(\frac{\partial u}{\partial r}\right)^2 = \rho \ell^2 \left(\frac{\partial u_d}{\partial r}\right)^2 \tag{121}$$

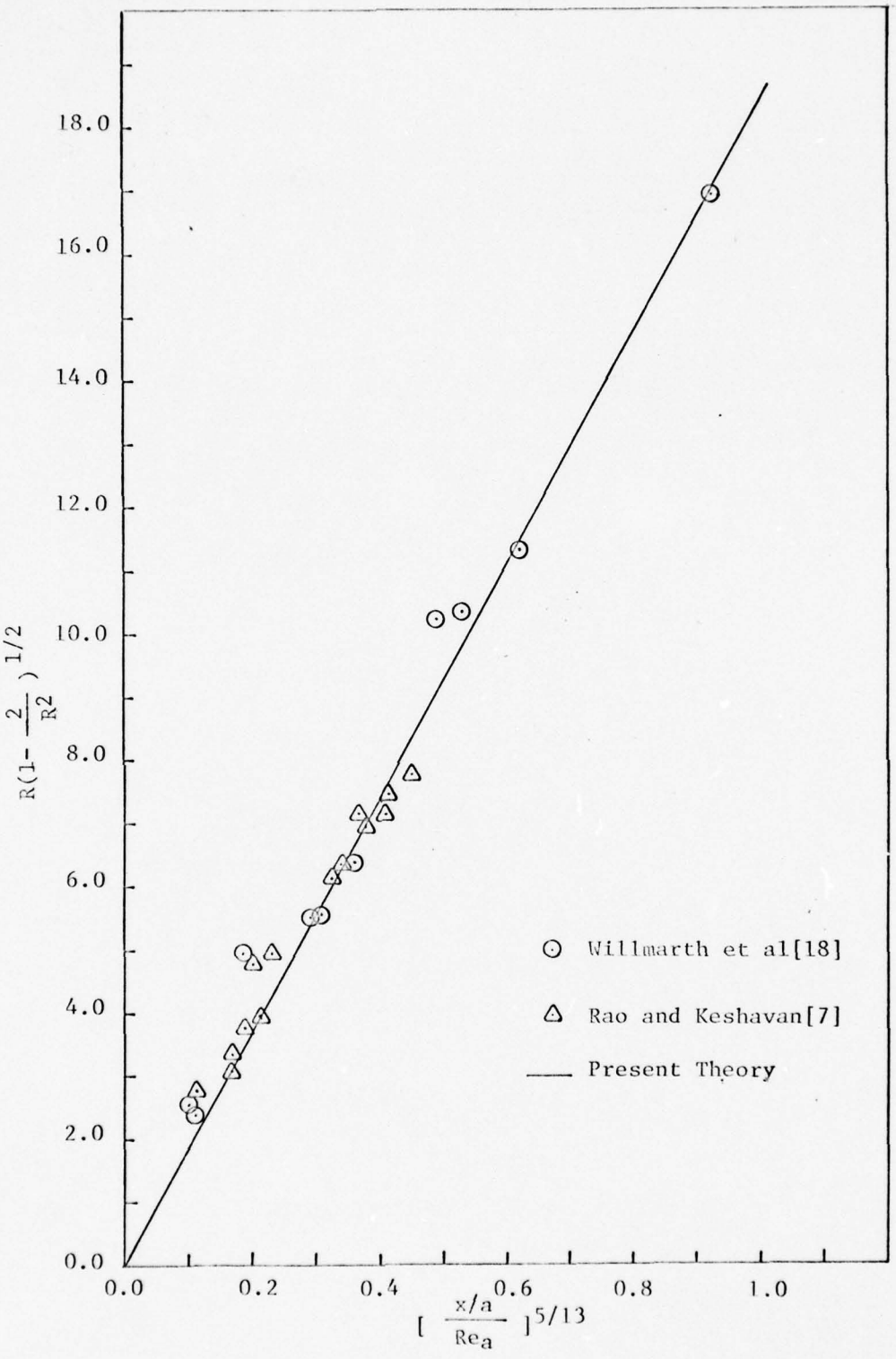

Figure 12. Boundary-Layer Thickness (Eddy-Viscosity Model)

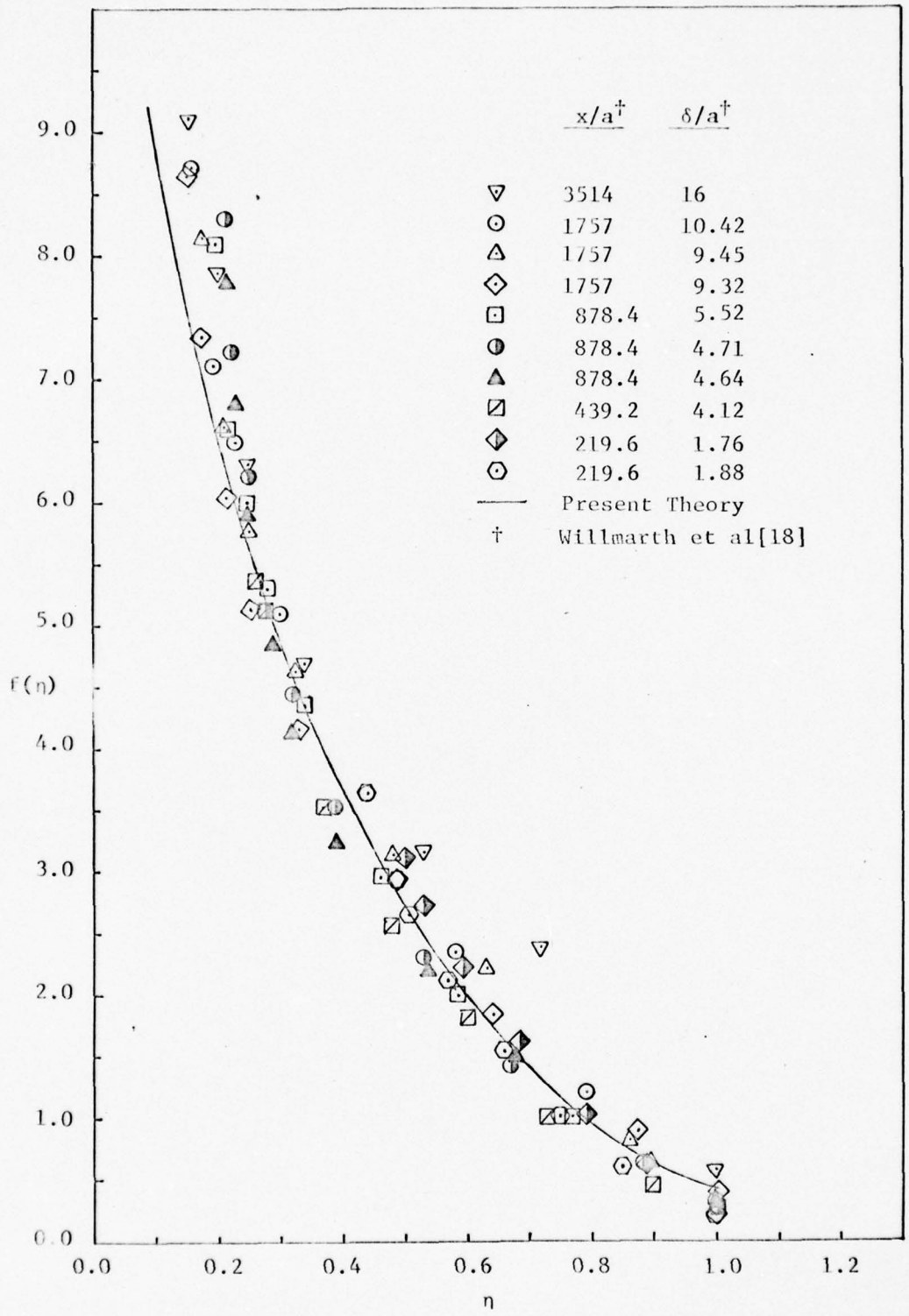

Figure 13. Velocity-Defect Law (Eddy-Viscosity Model)

In terms of the nondimensional quantities given in Eqs. (49) and (53), Eq. (121) becomes

$$\tau^+ = \lambda_\ell^2 \frac{U_e^2}{u_\tau^2 \, Re_a} \left(\frac{\partial \bar{u}_d}{\partial \eta}\right)^2 \tag{122}$$

or, by Eqs. (51) and (52),

$$\tau^+ = 2\lambda_\ell^2 \sqrt{Re_a} \, \beta^2 \, \chi^2 \, f'^2 \tag{123}$$

Equations (58) and (123) define the velocity-defect law. Substituting Eq. (123) into Eq. (58) and rearranging, one obtains

$$\frac{1}{2\lambda_\ell^2 \sqrt{Re_a}} \frac{\dot{R}}{\xi \chi} \left[\eta^2 f + \left(2 + \frac{R\dot{\chi}}{\dot{R}\chi}\right) \int_\eta^1 \eta f \, d\eta\right] = \eta f'^2 \tag{124}$$

The similarity assumption requires that

$$\frac{1}{2\lambda_\ell^2 \sqrt{Re_a}} \frac{\dot{R}}{\xi \chi} = \gamma \quad , \qquad \text{a constant} \tag{125}$$

and

$$2 + \frac{R\dot{\chi}}{\dot{R}\chi} = n \quad , \qquad \text{a constant} \tag{126}$$

Substituting the solution of Eq. (126), which was given previously by Eq. (65), with n = 2b, into Eq. (125) and separating the variables, one obtains

$$R^{2-n}\,\dot{R} = \frac{2\lambda_\ell^2 C}{\gamma}\sqrt{Re_a}\,\xi \tag{127}$$

Integration of Eq. (127), then gives

$$R^{3-n} + Q = \frac{\lambda_\ell^2 C(3-n)}{\gamma}\sqrt{Re_a}\,\xi^2 \tag{128}$$

where Q is a constant of integration. Combining the group of the constants into single constant and substituting the dimensional quantities, Eq. (128) yields the boundary-layer thickness in the form

$$R\left(1 + \frac{Q}{R^{3-n}}\right)^{\frac{1}{3-n}} = \bar{A}\left[\frac{x/a}{\sqrt{Re_a}}\right]^{\frac{1}{3-n}} \tag{129}$$

From Eq. (65)

$$\chi = \bar{B}\left[\frac{x/a}{\sqrt{Re_a}}\right]^{-\frac{2-n}{3-n}}\left(1 + \frac{Q}{R^{3-n}}\right)^{\frac{2-n}{3-n}} \tag{130}$$

Also, from Eq. (124), one obtains the equation for $f(\eta)$,

$$f'^2 = \gamma\eta f + \frac{n\gamma}{\eta}\int_\eta^1 \eta f\,d\eta \tag{131}$$

The transformation, $f(\eta) = \gamma F(\eta)$ reduces Eq. (131) to one with a single parameter

$$F'^2 = \eta F + \frac{n}{\eta}\int_\eta^1 \eta F\,d\eta \tag{132}$$

The boundary conditions are

$$\text{at} \quad \eta = 1 , \qquad F(1) = F'(1) = 0 \tag{133}$$

Exact solutions of Eq. (132) can easily be obtained for the values $n = 0$ and $n = 2$.

Case 1: $n = 0$

For $n = 0$, Eq. (132) reduces to

$$\frac{F'}{\sqrt{F}} = \sqrt{\eta} \tag{134}$$

Integration of Eq. (134) with the boundary condition of Eq. (133) gives the solution

$$F_o(\eta) = \frac{1}{9} (1 - \eta^{3/2})^2 \tag{135}$$

This solution with Eqs. (129) and (130) corresponds to that for an axisymmetric circular wake.

Case 2: $n = 2$

For $n = 2$, Eq. (132) becomes

$$\eta F'^2 = \eta^2 F + 2 \int_\eta^1 \eta F \, d\eta \tag{136}$$

Integrating by parts and using the boundary condition, Eq. (136) yields

$$\eta F'^2 = - \int_\eta^1 \eta^2 F' \, d\eta \tag{137}$$

Differentiation of Eq. (137) gives

$$F'(2\eta F'' + F' - \eta^2) = 0 \tag{138}$$

For $F' \neq 0$, $2\eta F'' + F' - \eta^2 = 0$ is a linear second-order differential equation, of which the general solution is

$$F_2(\eta) = C_1 + C_2 \eta^{1/2} + \frac{1}{15} \eta^3 \tag{139}$$

For $F' = 0$, $F_2(\eta) = C_3 = 0$, according to the boundary condition (133), an impossible solution. With the boundary conditions (133), the solution (139) becomes

$$F_2(\eta) = \frac{1}{15} (5 - 6\eta^{1/2} + \eta^3) \tag{140}$$

Let $\eta = (1 - z)^2$, then (141)

$$F_o(z) = z^2 \left(1 - 2z + \frac{5}{3} z^2 - \frac{2}{3} z^3 + \frac{1}{9} z^4\right) \tag{142}$$

$$F_2(z) = z^2 \left(1 - \frac{4}{3} z + z^2 - \frac{2}{3} z^3 + \frac{1}{15} z^4\right) \tag{143}$$

Here, the factor z^2 assures that the end conditions $F(0) = F'(0) = 0$ are satisfied.

The results for n = 0,2 suggest a solution for arbitrary values of n of the form

$$F(z) = \sum_{p=2}^{\infty} a_p z^p \tag{144}$$

Substitution of Eq. (141) into Eq. (132) gives

$$F'^2(z) = 4(1 - z)^4 F - 8n \int_z^o (1 - z)^3 F \, dz \tag{145}$$

Differentiating Eq. (145), one obtains

$$\frac{d}{dz} (F'^2) - 4(1 - z)^4 F' + 8(2 - n)(1 - z)^3 F = 0 \tag{146}$$

Put

$$\frac{d}{dz} (F'^2) = \sum_{p=1}^{\infty} A_p z^p \tag{147}$$

$$(1 - z)^4 F' = \sum_{p=1}^{\infty} B_p z^p \tag{148}$$

$$(1 - z)^3 F = \sum_{p=2}^{\infty} C_p z^p \tag{149}$$

Then Eq. (146) yields

$$A_1 = 4 B_1 \tag{150}$$

$$A_p = 4 B_p - 8(2 - n) C_p , \qquad p = 2,3,4,... \tag{151}$$

where, by Eqs. (147), (148) and (149)

$$A_p = \sum_{m=2}^{p+1} (p + 1) m(p - m + 3) a_m a_{p-m+3} \tag{152}$$

$$B_p = (p+1)a_{p+1} - 4p\,a_p + 6(p-1)a_{p-1} - 4(p-2)a_{p-2} + (p-3)a_{p-3} \tag{153}$$

$$C_p = a_p - 3a_{p-1} + 3a_{p-2} - a_{p-3} \tag{154}$$

Then, from Eq. (150)

$$8a_2^2 = 8a_2 \tag{155}$$

and hence $a_2 = 0$ or 1. From Eq. (151)

$$\sum_{m=2}^{p+1} (p+1)m\ \ (p-m+3)a_m\, a_{p-m+3} = 4(p+1)a_{p+1} - 8\,(2p+2-n)a_p$$

$$+ 24(p+1-n)a_{p-1} - 8(2p+2-3n)a_{p-2} + 4(p+1-2n)a_{p-3} \tag{156}$$

$$p = 2,3,4,\ldots$$

If $a_2 = 0$, then from Eq. (156), $a_3 = a_4 = \ldots = 0$ also, a trivial solution. Hence, $a_2 = 1$. From. Eq. (156), for

$$p = 2 \qquad a_3 = -\frac{1}{3}\,(6-n) \tag{157}$$

$$p = 3 \qquad a_4 = \frac{1}{36}\,(60 - 10n - n^2) \tag{158}$$

$$p = 4 \qquad a_5 = -\frac{1}{90}\,(60 - 16n + 4n^2 - n^3) \tag{159}$$

For $p = 6,7,8,9,\ldots$, the a_p's can be successively obtained from

$$a_{p+1} = -\frac{1}{4p}\sum_{m=3}^{p} m(p-m+3)a_m\, a_{p-m+3} - \frac{2}{p(p+1)}(2p+2-n)a_p$$

$$+\frac{6}{p(p+1)}(p+1-n)a_{p-1} - \frac{2}{p(p+1)}(2p+2-3n)a_{p-2}$$

$$+\frac{1}{p(p+1)}(p+1-2n)a_{p-3} \qquad (160)$$

Therefore, the solution of Eq. (132) is the series given by Eq. (144) with the coefficients given by Eqs. (157), (158), (159) and (160). For n = 0 and n = 2, this series solution gives exactly a sixth-degree polynomial. For other values of n in the range $0 < n < 2$ the series behaves as a semi-convergent one, which, if also truncated at the sixth degree in z, gives results in excellent agreement with step-by-step numerical solutions of the differential equation. Figure 14 compares the numerical solution of Eq. (132) and the series solution with six terms for various values of n. Then, from Eq. (160), for p = 5,

$$a_6 = \frac{1}{8100}(900 + 168n - 596n^2 + 299n^3 - 44n^4) \qquad (161)$$

Thus the solution is given, with sufficient accuracy, by

$$F(z) \approx z^2\left[1 - \frac{1}{3}(6-n)z + \frac{1}{36}(60-10n-n^2)z^2 - \frac{1}{90}(60-16n+4n^2-n^3)z^3\right.$$

$$\left.+\frac{1}{8100}(900+168n-596n^2+299n^3-44n^4)z^4\right] \qquad (162)$$

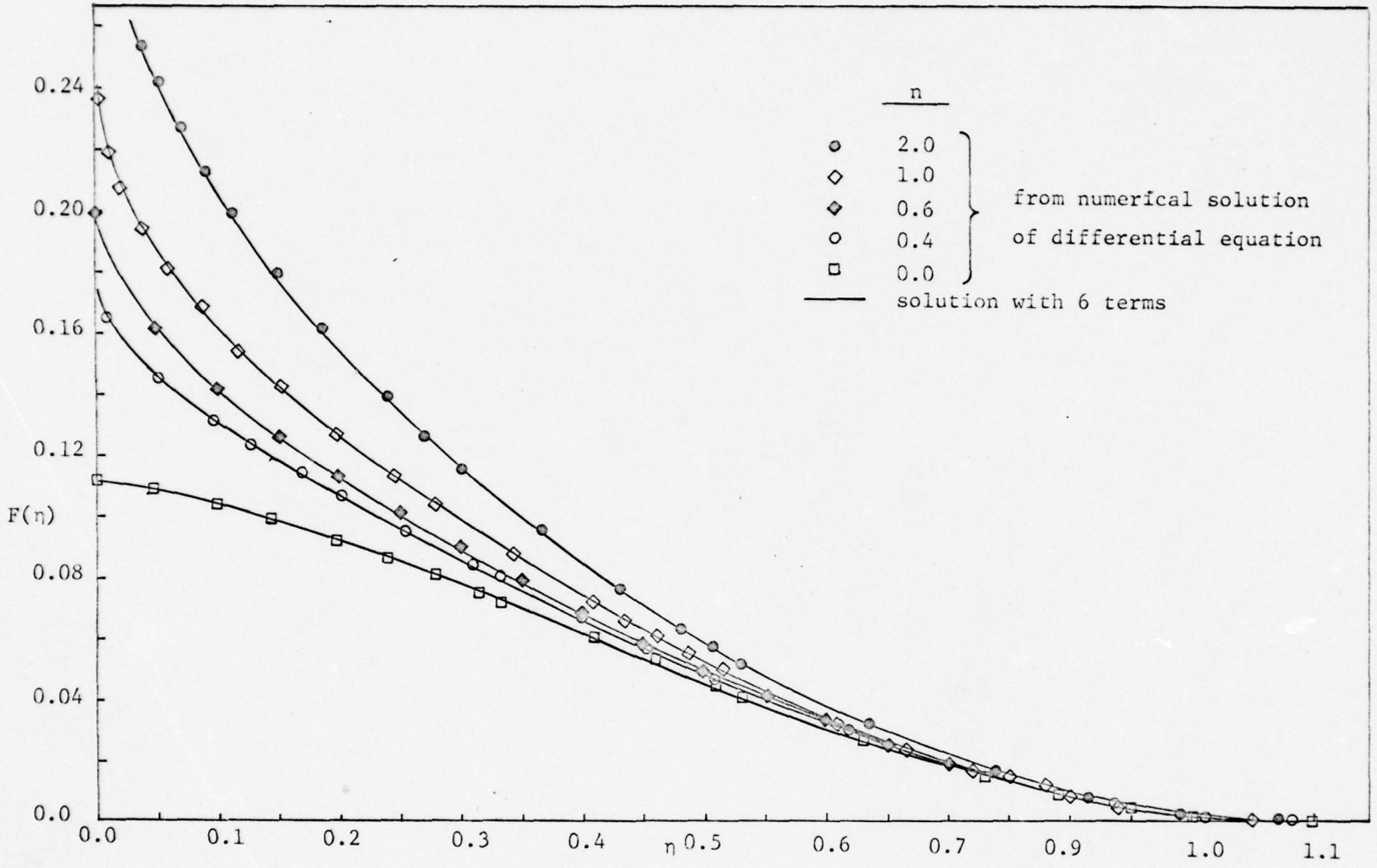

Figure 14. Comparison of Series Solution with 6 Terms with Numerical Solution of Differential Equation
(Mixing-Length Model)

From Eqs. (49), (52) and (130), we obtain

$$\frac{U_e - u}{U_e} = \frac{\bar{B}}{\sqrt{Re_a}} \left[\frac{x/a}{\sqrt{Re_a}}\right]^{-\frac{2-n}{3-n}} \left(1 + \frac{Q}{R^{3-n}}\right)^{\frac{2-n}{3-n}} F(z) , \quad \eta = (1-z)^2 \tag{163}$$

Equations (129) and (163) contain 4 undetermined constants, namely n, $\bar{A}$, $\bar{B}$ and Q. The value of $n = 2b = 0.7$, was determined previously in Sec. 2.3. Also, the value of Q can be estimated by using the results of the previous section. From Eq. (68), for small values of ξ, R goes asymptotically to $\sqrt{2}$, a value of R which might be considered to give the virtual origin. Therefore, from Eq. (128), as ξ goes to zero, the value of Q is given by $Q = -R^{3-n} = -(\sqrt{2})^{2.3} = 2.2$. The value of $\bar{A}$ was determined by plotting $\left[\frac{x/a}{Re_a}\right]^{\frac{1}{3-n}}$ versus $R\left(1 - \frac{2.2}{R^{3-n}}\right)^{\frac{1}{3-n}}$. The slope gave $\bar{A} = 3$. In order to find the value of $\bar{B}$, let

$$Y = \frac{U_e - u}{U_e} \sqrt{Re_a} \left[\frac{x/a}{\sqrt{Re_a}}\right]^{\frac{2-n}{3-n}} \left(1 - \frac{2.2}{R^{3-n}}\right)^{-\frac{2-n}{3-n}} , \quad n = 0.7 \tag{164}$$

$$Z = F(z) , \quad \eta = (1 - z)^2 \tag{165}$$

Then Eq. (163) can be written as

$$Y = \bar{B}Z \tag{166}$$

The values of Y obtained from Willmarth's data were plotted against the values of F(z) obtained from Eq. (162) with n = 0.7, corresponding to the same value of z. The results plotted along a straight line, but the line did not pass through the origin. This discrepancy is due to an ill-defined boundary-layer thickness. Theoretically, as $\eta = \frac{y + a}{\delta + a} \to 1$ (as $y \to \infty$), $\frac{U_e - u}{U_e} = 0$. But, for practical purposes, δ is defined as the value of y where $\frac{Ue - u}{U_e} = 0.01$. Therefore, Eq. (166) needs to be corrected to

$$Y = \bar{B} Z + \bar{C} \quad ,$$

where $\bar{C}$ = constant.

From the slope and intercept of the plot of Eq. (166), the values of $\bar{B}$ and $\bar{C}$ are

$$\bar{B} = 618$$

$$\bar{C} = 4.5$$

In summary, the results are

$$R\left(1 - \frac{2.2}{R^{3-n}}\right)^{\frac{1}{3-n}} = 3\left(\frac{x/a}{\sqrt{Re_a}}\right)^{\frac{1}{3-n}} \tag{167}$$

$$\frac{U_e - u}{U_e} = \frac{1}{\sqrt{Re_a}}\left[\frac{x/a}{\sqrt{Re_a}}\right]^{-\frac{2-n}{3-n}}\left(1 - \frac{2.2}{R^{3-n}}\right)^{\frac{2-n}{3-n}}[618F(z) + 4.5] \tag{168}$$

$$\eta = (1 - z)^2 \quad , \qquad n = 0.7$$

$$F(z) \approx z^2 \left[1 - \frac{53}{30} z + \frac{35}{24} z^2 - \frac{5}{9} z^3 + \frac{1}{10} z^4\right] \tag{169}$$

Equation (169) has been obtained from Eq. (162) by substituting $n = 0.7$. The comparison with Willmarth's data is shown in Figs. 15 and 16.

The comparison of Fig. 13 and Fig. 15 reveals that eddy-viscosity model yields a better correlation of the data than the mixing-length model. Consequently, the eddy-viscosity model was selected in the subsequent analysis.

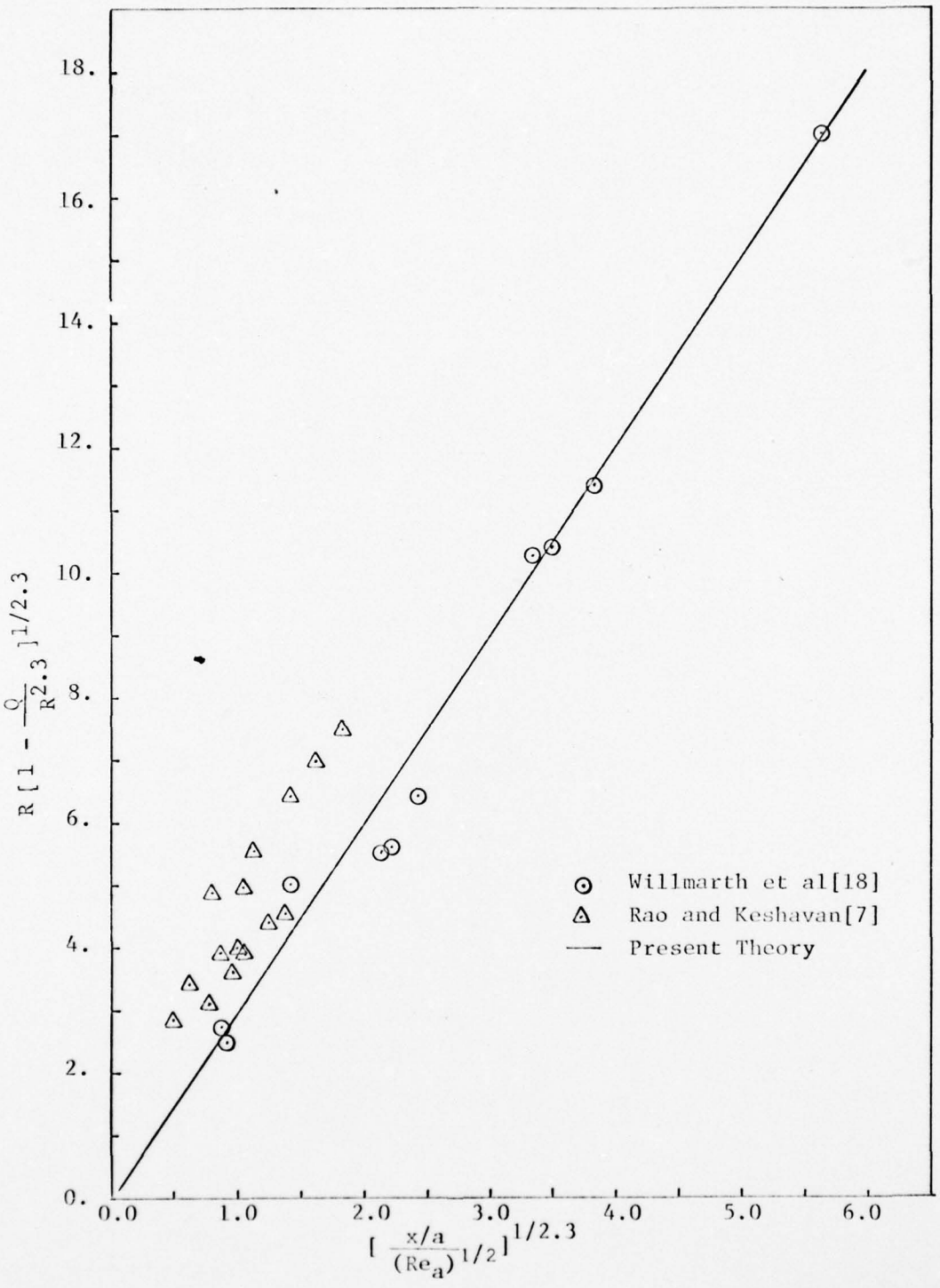

Figure 15. Boundary-Layer Thickness (Mixing-Length Model)

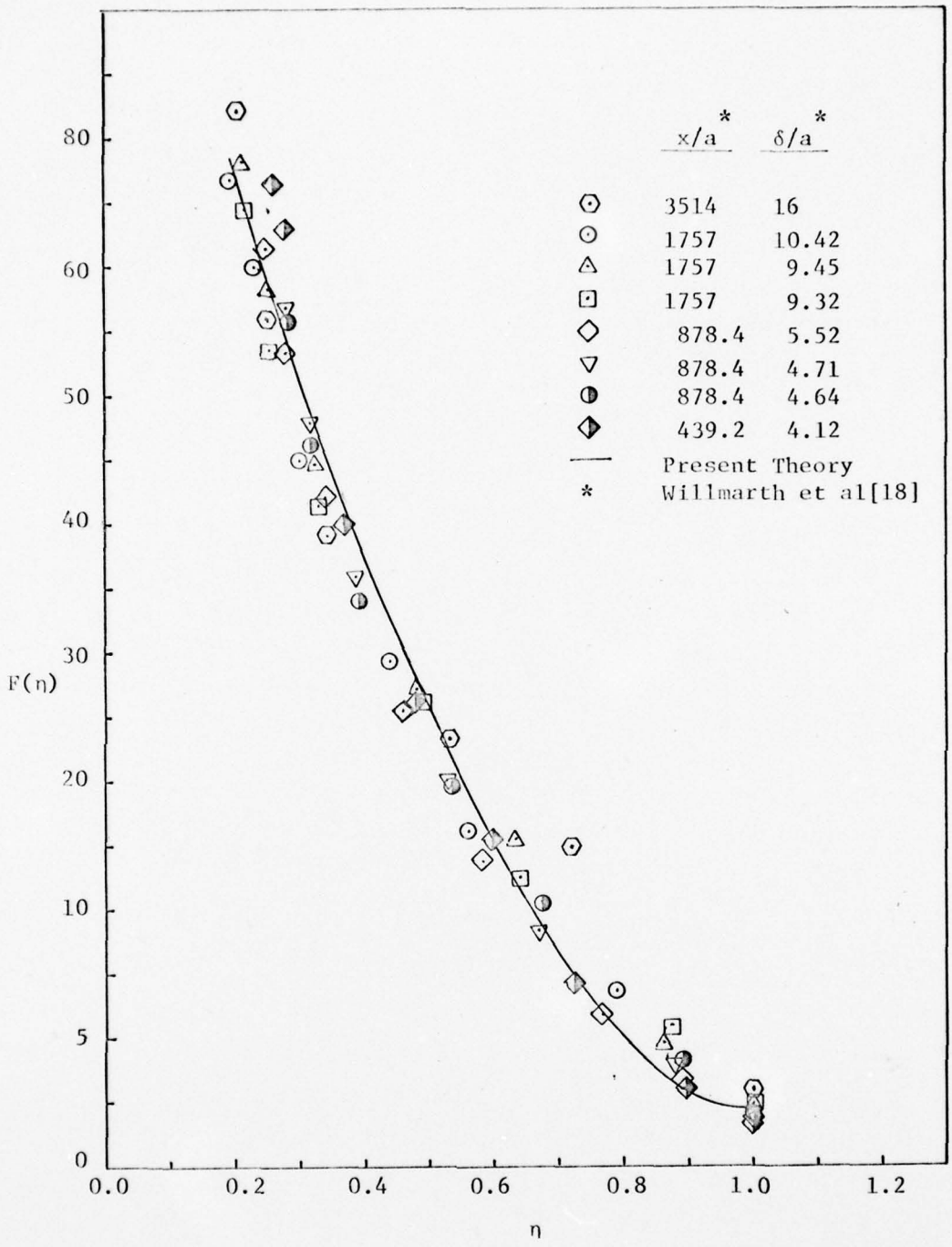

Figure 16. Velocity-Defect Law (Mixing-Length Model)

CHAPTER 3

RESULTS AND DISCUSSION

3.1 Boundary-Layer Characteristics

3.1.1 Velocity Profiles

Two similarity laws for a thick, axisymmetric, turbulent boundary layer growing on a long, circular cylinder of constant radius have been established. As for the boundary layer on a flat plate, these are the law of the wall and the velocity-defect law.

In Chapter 1, it has been shown that the logarithmic mixing length, rather than the linear one, gives a better modeling of the Reynolds stresses for axisymmetric turbulent flows with zero pressure gradient. Also, it has been shown that the logarithmic mixing length gives the usual log region in terms of the Exponential Integral of $\ell n\sqrt{1 + y/a}$. This has a series expansion in terms of the argument, $Y^* = a^*\sqrt{1 + y^*/a^*}\ \ell n(1 + y^*/a^*)$, which behaves like y^* for $y/a \leq 1$. This result explains why the cylinder data, when plotted in terms of two-dimensional coordinates, as was done by Willmarth et al. [18], do not deviate appreciably from flat-plate results. It also verifies the use of a Preston tube to measure the wall shear stress for axisymmetric boundary layers.

As can be seen from Fig. 9 , the logarithmic region extends farther to larger values of y^* as a^* increases. It also verifies that $a^* = au_\tau/\nu$, which is a measure of the effect of transverse curvature,

is an important parameter for scaling the velocity distribution in the law-of-the-wall region.

In Chapter 2, a similarity solution has been obtained analogous to an axisymmetric wake in the velocity-defect region. The results show that the velocity-defect profiles can be scaled by using two parameters, x/a and $R = \delta + a$. In order to expect the boundary layer to act like a wake, δ/a has to be large compared to unity, which, in turn, is a result of the transverse-curvature effect. Willmarth's data verify that the portion of the boundary layer which acts like a wake becomes larger as δ/a increases. The limiting case, that of a flat-plate boundary layer, $(a \to \infty)$ is thus excluded from consideration.

In the case of the flat-plate boundary layer, the logarithmic parts of the law of the wall and the velocity-defect law can be obtained by assuming that there is an overlapping region in which both laws are valid. For the cylinder, however, the assumptions made to obtain the solutions fail at the limits of the law of the wall and the velocity-defect law. In the law-of-the-wall region, it is assumed that the stress moment is constant. Hence the shear stress is given by $\tau^+ = /(a+y)$, which ignores the inertia terms in the mean-flow momentum equation. For large values of y^*, however, the inertia terms are no longer negligible. Furthermore, in the derivation of the velocity-defect law, it is assumed that Oseen's approximation is valid, and that the velocity gradient $\partial u/\partial y$ and the radial velocity v are small. On the contrary, as η becomes small, both of these assumptions fail. Hence, the overlapping of the inner and the

outer laws, which requires continuity of the velocity gradient $\partial u/\partial y$, and consequently the continuity of the shear stress which depends on the velocity gradient $\partial u/\partial y$ through phenomenological relations, does not occur. However, the velocity profiles calculated from the law of the wall and the velocity-defect law do intersect each other at an angle which decreases as Re_a increases. Figs. 17-19 compare the velocity profiles calculated from theory with the Willmarth data. As can be seen from these plots, the agreement is quite good except near the intersection point. Willmarth's data reveal that the intersection occurs at about $y/(\delta + a) = 0.125$. For all practical purposes, the velocity profiles can be predicted using the law of the wall and the velocity-defect law, and should be smoothed by a french curve near the intersection point.

3.1.2 Estimation of the Wall Shear Stress

For the flat-plate boundary layer, the overlapping concept plays an important role in deriving a skin-friction law. Since there is no overlapping region for the present problem, a similar procedure for obtaining a skin-friction formula is not possible. For all practical purposes, however, the wall-shear stress can be determined from the intersection of the two laws, by an iterative procedure.

The velocity-defect law gives the velocity profile, up to the intersection point, by Eq. (119). After dividing and multiplying by $\sigma = U_e/u_\tau$ at the intersection point, Eq. (119) becomes

$$\sigma - u^*(\bar{r}_c) = 4\sigma\sqrt{\frac{a}{x}}\left(1 - \frac{2}{R^2}\right)^{0.65} e^{-z_c} U(b,1,z_c) \qquad (170)$$

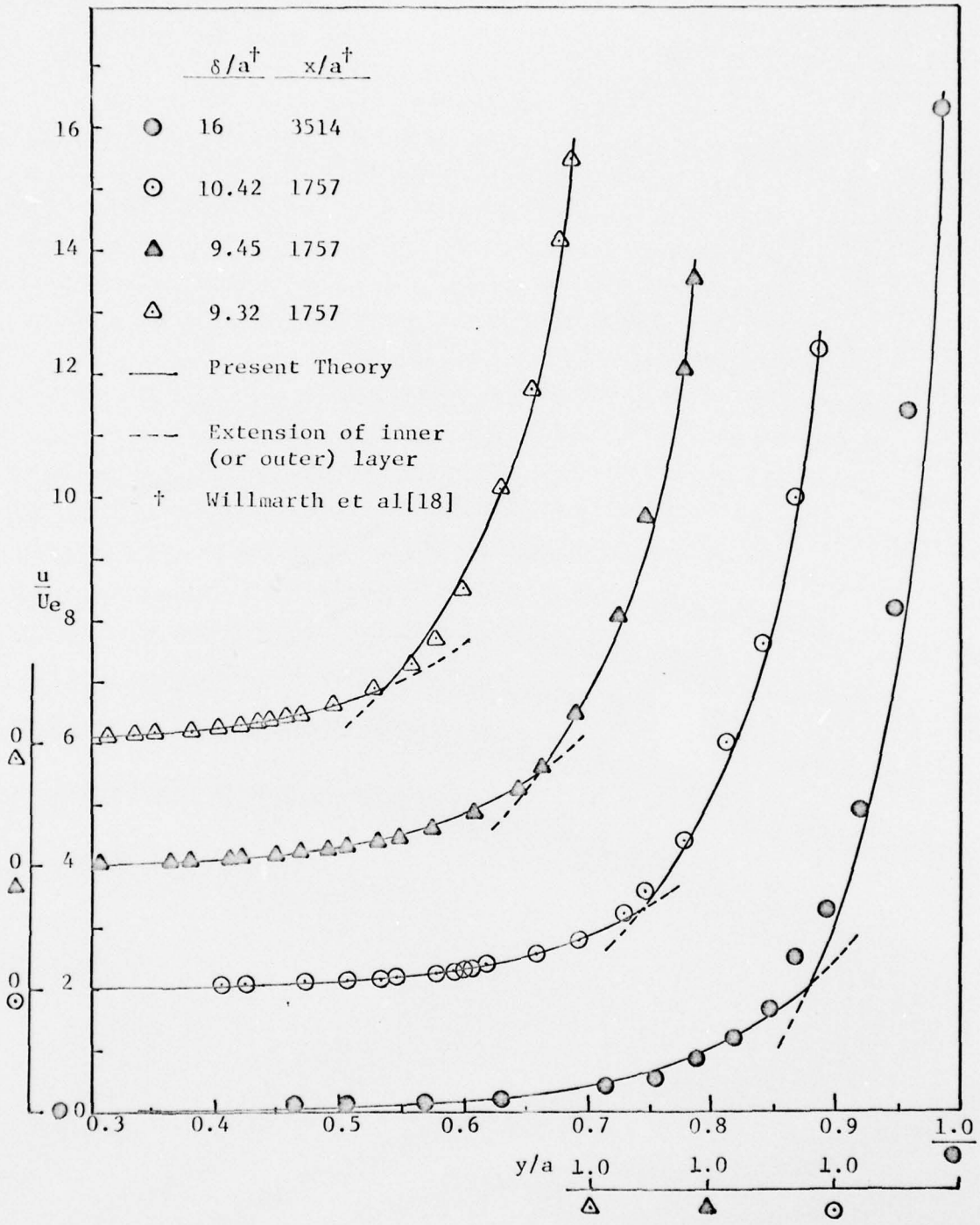

Figure 17. Comparison of Velocity Profiles

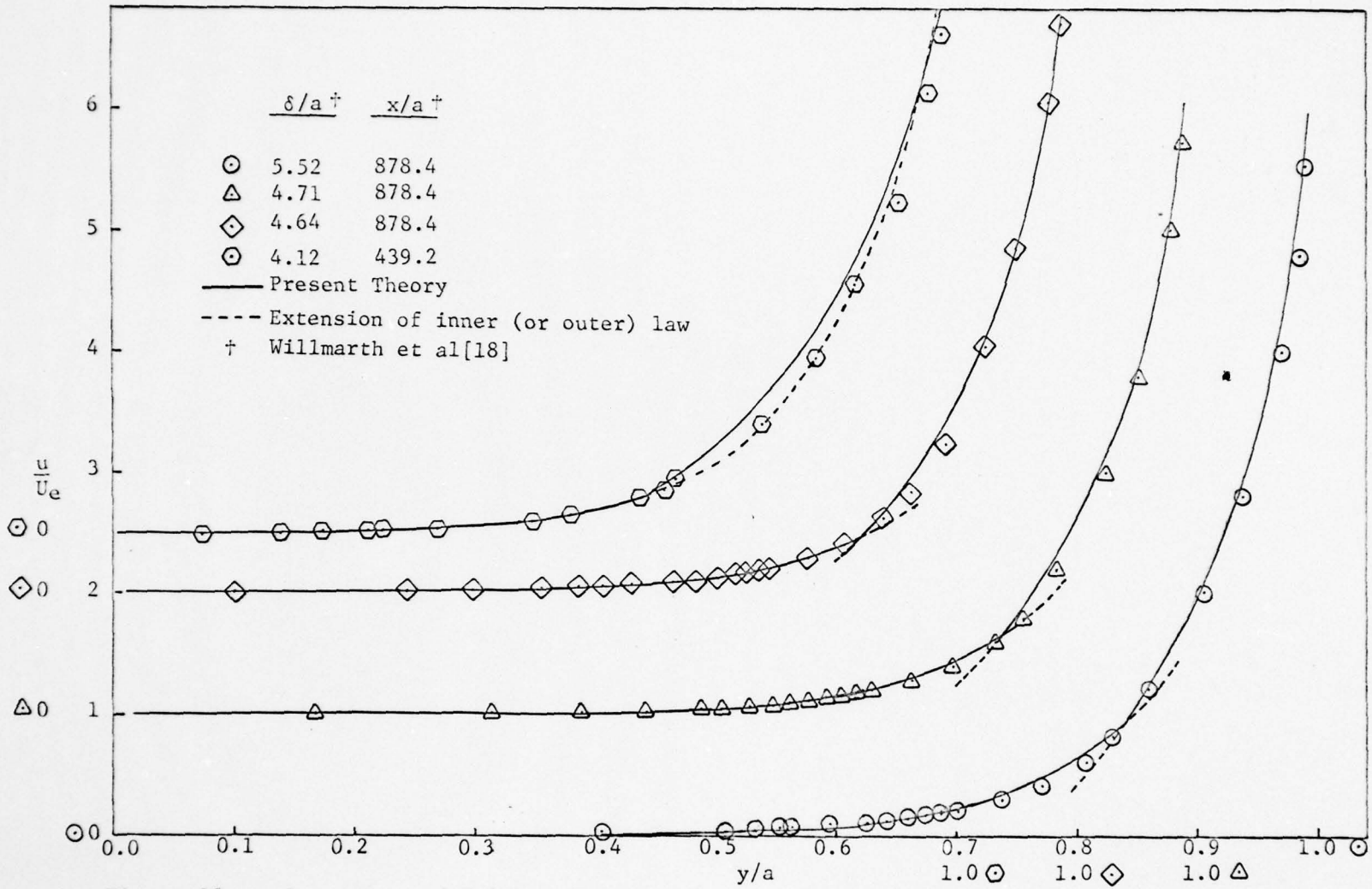

Figure 18. Comparison of Velocity Profiles

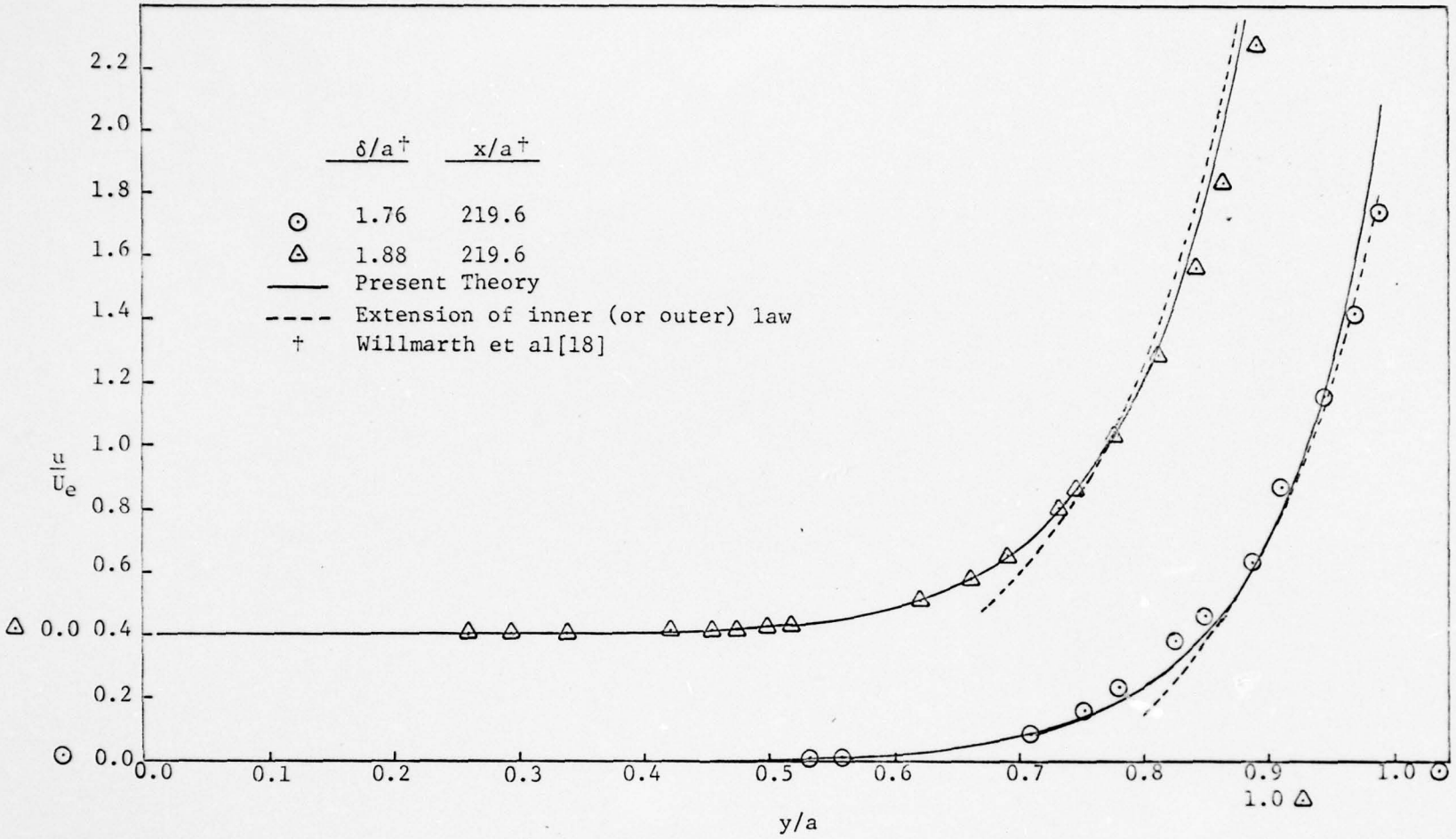

Figure 19. Comparison of Velocity Profiles

where $z_c = 2\eta_c^2 = 2\,\dfrac{r_c^2}{(\delta + a)^2}$ is the point at which the two laws intersect, indicated by the subscript c. From Eqs. (37), (41) and (44), with $a^* = \dfrac{Re_a}{\sigma}$, we have

$$u^*(\bar{r}_c) = \frac{1}{\kappa} E_i[\ln\sqrt{\bar{r}_c}] + \frac{1}{\kappa} \ln 2\,\frac{Re_a}{\sigma} + 5.45 - \frac{41.76}{Re_a}\,\sigma - \frac{\gamma}{\kappa} \tag{171}$$

Substituting Eq. (171) into Eq. (170) and rearranging gives

$$\sigma H + \frac{1}{\kappa} \ln\sigma = P \tag{172}$$

where

$$H = 1 + \frac{41.76}{Re_a} - 4\sqrt{\frac{a}{x}}\left(1 - \frac{2}{R^2}\right)^{0.65} e^{-z_c}\, U(b,1,z_c) \tag{173}$$

$$P = 5.45 + \frac{1}{\kappa}\left\{E_i[\ln\sqrt{\bar{r}_c}] + \ln 2Re_a - \gamma\right\} \tag{174}$$

Given the values of x/a and Re_a, $R = (\delta + a)/a$ can be computed from Eq. (118) and consequently, z_c, $\bar{r}_c$, H and P. Therefore σ can be computed by the iteration formula

$$\sigma_i = \frac{1}{H}\left(P - \frac{1}{\kappa} \ln \sigma_{i-1}\right) \tag{175}$$

Table 3.1 compares the results computed by using the above procedure with Willmarth's measured values, and the values of σ obtained from a Clauser plot.

TABLE 3.1 COMPARISON OF σ VALUES

x/a	Re_a	δ/a	σ_m (Measured)	σ_c (Computed)	σ_{cp} (Clauser Plot)	% Error $\left\lvert\frac{\sigma_m - \sigma_c}{\sigma_n}\right\rvert$	% Error $\left\lvert\frac{\sigma_c - \sigma_{cp}}{\sigma_{cp}}\right\rvert$
3514	4330	16.2	21.85	22.30	21.85	2.06	2.06
1757	6203	10.42	22.81	22.97	22.85	0.7	0.53
1757	9494	9.45	24.45	23.76	23.84	2.74	0.34
1757	11693	9.32	25.61	24.26	23.62	5.27	2.71
878.4	12790	5.52	24.91	23.98	24.08	3.73	0.42
878.4	19230	4.71	25.60	24.41	24.30	4.65	0.45
878.4	23100	4.64	25.92	24.82	24.27	4.25	2.27
439.2	36680	4.12	26.96	27.30	26.65	1.26	2.44
219.6	74260	1.76	27.41	26.02	26.21	5.07	0.72
219.6	92310	1.88	29.23	26.99	27.26	7.66	0.99

3.1.3 Shear-Stress Distribution

The distribution of the shear stress, as discussed in Section 1.2, can be approximated by $\tau^+ = a/(a + y)$ in the law-of-the wall region. In the velocity-defect region, the shear-stress distribution in terms of the eddy viscosity is given by Eq. (61),

$$\tau^+ = - \frac{\varepsilon}{\nu} \frac{\sigma^2}{Re_a^{3/2}} \frac{\chi}{R} f' \tag{176}$$

where

$$f' = \frac{df}{d\eta} = \frac{d}{dz} [e^{-z} U(b,1,z)] \frac{dz}{d\eta} = - e^{-z} U(b,2,z) \frac{\sqrt{2z}}{\alpha} \tag{177}$$

Substituting Eqs. (113), (118) and (177) and the values of the constants determined previously into Eq. (176), one obtains

$$\tau^+ = \frac{370}{13\sqrt{2}} \frac{\sigma^2}{Re_a^{3/2}} \left(\frac{x/a}{Re_a}\right)^{-\frac{29}{26}} \left(1 - \frac{2}{R^2}\right)^{1.15} \sqrt{z}\, e^{-z} U(b,2,z) \tag{178}$$

Figures 20 and 21 show the shear-stress distribution computed from Eqs. (17) and (178) for two sets of Willmarth's data. Around the point of intersection of two laws, there is a discontinuity in the shear-stress distribution. As discussed in Section 3.1.1, this is due to the invalidity of the assumptions made in obtaining the solutions for the law of the wall and the velocity-defect law in the neighborhood of $y/(\delta + a) \approx 0.125$. For an axisymmetric, thick turbulent boundary layer, the velocity profiles are much fuller compared

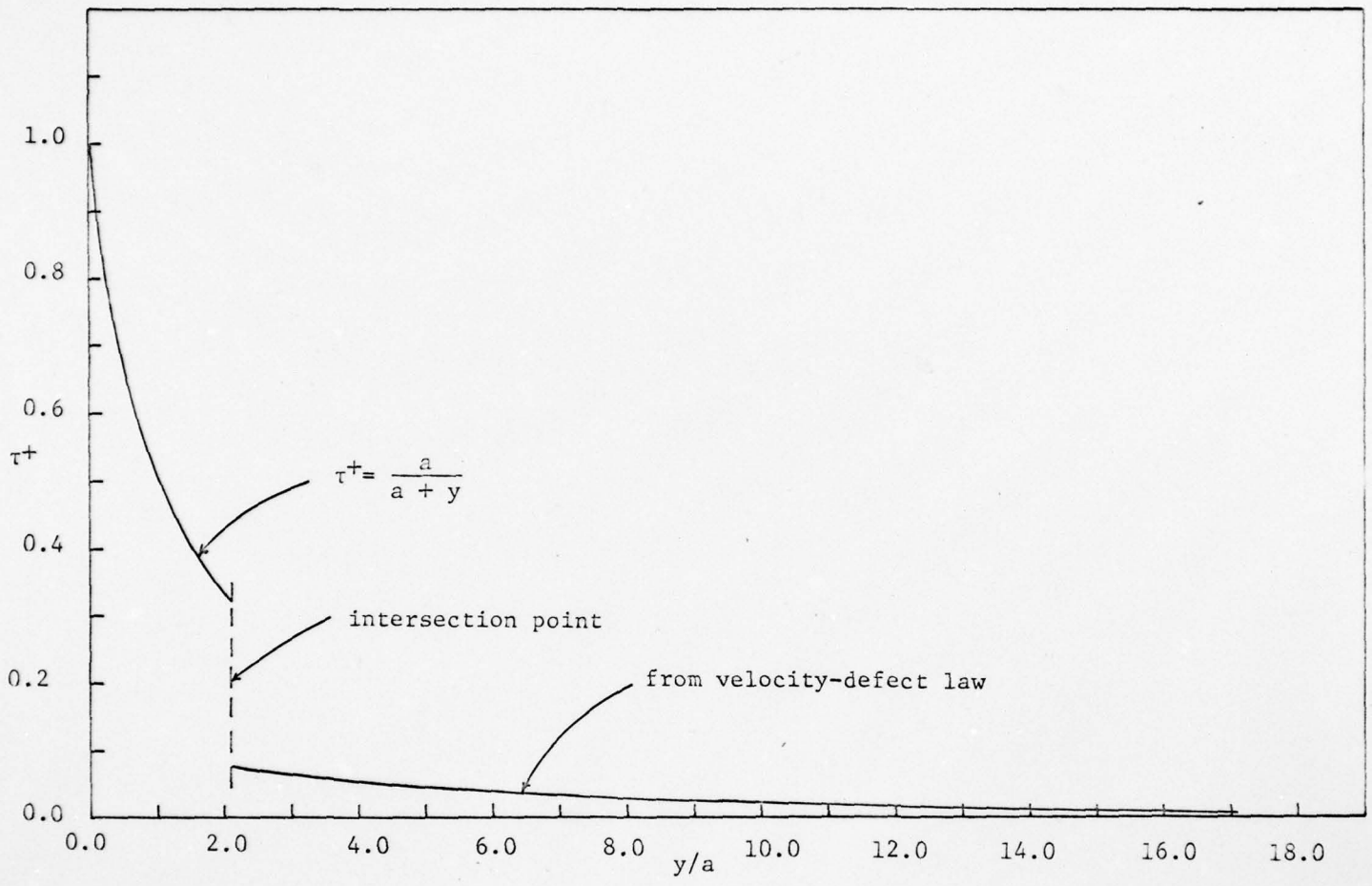

Figure 20. Shear-Stress Distribution for $\delta/a = 16$, $a^* = 198.2$

AD-A065 443 IOWA INST OF HYDRAULIC RESEARCH IOWA CITY F/G 20/4
AN ANALYTICAL SOLUTION OF THE THICK AXISYMMETRIC TURBULENT BOUN--ETC(U)
DEC 78 N DENLI N00014-75-C-0273
NL

UNCLASSIFIED

2 OF 2
AD
A065443

END
DATE
FILMED
4 -79
DDC

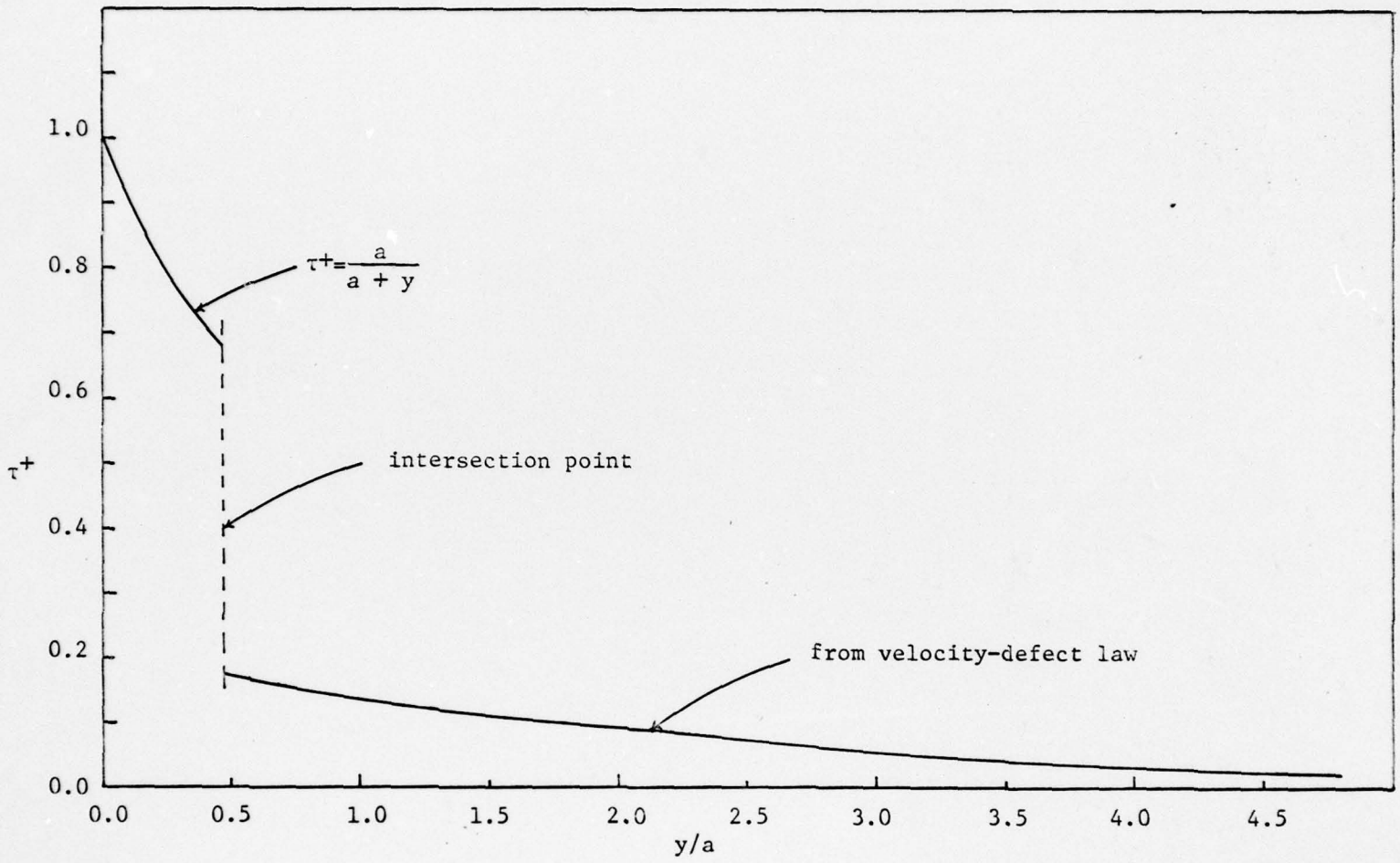

Figure 21. Shear-Stress Distribution for $\delta/a = 4.71$, $a^* = 791.5$

to those of thin boundary layers. The axisymmetric, thick, turbulent boundary layer profiles make an almost 90 degree turn at about $y/(\delta + a) = 0.125$. Thus, the classical, phenomenological theories which relate the shear-stress distribution to the velocity gradient $\partial u/\partial y$, through either a mixing-length or eddy-viscosity concept, fail to give a complete description of the shear-stress distribution if the usual inner- and outer-layer concepts are used. Apparently, there is a third region between these layers which would have to be determined if more accurate and continuous shear-stress distributions are required.

3.1.4 Displacement and Momentum Thicknesses

The usual definitions of the displacement and momentum thickness for an axisymmetric boundary layer flow are

$$\delta_1 = \int_a^{a+\delta} \left(1 - \frac{u}{U_e}\right) \frac{r}{a}\, dr \tag{179}$$

and

$$\theta_1 = \int_a^{a+\delta} \frac{u}{U_e} \left(1 - \frac{u}{U_e}\right) \frac{r}{a}\, dr \tag{180}$$

Kelly [2], in 1954, showed that if the boundary layer is thick, the displacement and the momentum thicknesses require new definitions for cylindrical flow, and the physically coherent definitions are

$$(\delta^* + a)^2 - a^2 = \int_a^{a+\delta} \left(1 - \frac{u}{U_e}\right) dr^2 \tag{181}$$

and

$$(\theta + a)^2 - a^2 = \int_a^{a+\delta} \frac{u}{U_e} \left(1 - \frac{u}{U_e}\right) dr^2 \tag{182}$$

The displacement thickness δ^* and the momentum thickness θ are related to the displacement length δ_1 and the momentum length θ_1 by

$$\delta_1 = \delta^* \left(1 + \frac{\delta^*}{2a}\right) \tag{183}$$

$$\theta_1 = \theta \left(1 + \frac{\theta}{2a}\right) \tag{184}$$

If $\bar{r}_c$ is the intersection point where the law of the wall and the velocity-defect law intersect, then Eqs. (179) and (180) can be split into two integrals to be evaluated accordingly,

$$\frac{\delta_1}{a} = \int_1^{\bar{r}_c} \left(1 - \frac{u}{U_e}\right) \bar{r}\, d\bar{r} + \int_{\bar{r}_c}^{R} \left(1 - \frac{u}{U_e}\right) \bar{r}\, d\bar{r} \tag{185}$$

or

$$\frac{\delta_1}{a} = \frac{1}{2}\left(\bar{r}_c^2 - 1\right) - I_1 + I_2 \tag{186}$$

where

$$I_1 \equiv \frac{1}{\sigma} \int_1^{\bar{r}_c} u^* \bar{r}\, d\bar{r} \tag{187}$$

$$I_2 \equiv \int_{\bar{r}_c}^{R} \left(1 - \frac{u}{U_e}\right) \bar{r}\, d\bar{r} \tag{188}$$

Also, Eq. (180) gives

$$\frac{\theta_1}{a} = I_1 - I_3 + \int_{\bar{r}_c}^{R} \left(1 - \frac{u_d}{U_e}\right) \frac{u_d}{U_e} \; \bar{r} \; d\bar{r} \tag{189}$$

where

$$I_3 = \frac{1}{\sigma^2} \int_1^{\bar{r}_c} u^{*2} \; \bar{r} \; d\bar{r} \tag{190}$$

Since, the term $\left(\frac{u_d}{U_e}\right)^2$ is very small in the velocity-defect region, it can be neglected in the integral in Eq. (189). Hence

$$\frac{\theta_1}{a} = I_1 + I_2 - I_3 \tag{191}$$

Integrating Eq. (187) by parts and using the nonslip condition, $u^*(1) = 0$, gives

$$I_1 = \frac{1}{2\sigma} \left\{ \bar{r}_c^2 \; u^*(\bar{r}_c) - \int_1^{\bar{r}_c} \frac{\partial u^*}{\partial \bar{r}} \; \bar{r}^2 \; d\bar{r} \right\} \tag{192}$$

Since,

$$\bar{r} = 1 + \frac{y}{a} = 1 + \frac{y^*}{a^*} \quad , \qquad \frac{\partial u^*}{\partial \bar{r}} = \frac{\partial u^*}{\partial y^*} \; \frac{\partial y^*}{\partial \bar{r}} = a^* \; \frac{\partial u^*}{\partial y^*} \tag{193}$$

Also, in the log-region, Eq. (35) gives

$$\frac{\partial u^*}{\partial y^*} = \frac{1}{\kappa} \; \frac{1}{\sqrt{\bar{r}} \; \ell n \bar{r}} \tag{194}$$

Substituting Eqs. (193) and (194) into Eq. (192), we obtain

$$I_1 = \frac{1}{2\sigma}\left\{\bar{r}_c^2\, u^*(\bar{r}_c) - \int_1^{\bar{r}_1} \frac{\partial u^*}{\partial \bar{r}}\, \bar{r}^2\, d\bar{r} - \frac{1}{\kappa}\int_{\bar{r}_1}^{\bar{r}_c} \frac{\bar{r}^{3/2}\, d\bar{r}}{\ell n \bar{r}}\right\} \qquad (195)$$

where $\bar{r}_1 = 1 + \frac{63}{a^*}$, is the point where the fully turbulent region begins. The change of variables $t = \bar{r}^{5/2}$ yields

$$I_1 = \frac{1}{2\sigma}\left\{\bar{r}_c^2\, u^*(\bar{r}_c) - \frac{1}{\kappa}\left(E_i[\ell n \bar{r}_c^{5/2}] - E_i[\ell n \bar{r}_1^{5/2}]\right) - \int_1^{\bar{r}_1} \frac{\partial u^*}{\partial \bar{r}}\, \bar{r}^2\, dr\right\} \qquad (196)$$

In Eq. (196), $u^*(\bar{r}_c)$ is given by Eq. (42) in Chapter 1, and the integral can be computed by a suitable numerical scheme with $\partial u^*/\partial \bar{r}$ obtained from Eq. (34).

The integrand of Eq. (188) is given by Eq. (119). Hence substituting $z = 2\eta^2 = 2\frac{\bar{r}^2}{R^2}$, or $\bar{r}\, d\bar{r} = \frac{R^2}{4}\, dz$ reduces Eq. (188) to

$$I_2 = \sqrt{\frac{a}{x}}\left(1 - \frac{2}{R^2}\right)^{0.65} R^2 \int_{z_c}^{2} e^{-z}\, U(b,1,z)dz \quad , \quad z_c = \frac{2\bar{r}_c^2}{R^2} \qquad (197)$$

The integral in Eq. (197) is given by Magnus, Oberhettinger and Soni [22]. Therefore,

$$I_2 = \sqrt{\frac{a}{x}}\left(1 - \frac{2}{R^2}\right)^{0.65} R^2\left[e^{-z_c}\, z_c\, U(b+1,2,z_c) - 2e^{-2}\, U(b+1,2,2)\right] \qquad (198)$$

The integral I_3, given by Eq. (190) must be evaluated by a numerical method with u^* obtained from Eq. (34).

Table 3.2 compares the displacement and the momentum thicknesses, computed by using the above relations, with Willmarth's data. In the computations, Simpson's 1/3 rule was used for the numerical integrations. The agreement is seen to be good except for the last three conditions. A possible explanation for the discrepancy for these conditions is that the flow was not axisymmetric for these cases, as was indicated by Willmarth et al[18].

TABLE 3.2 COMPARISON OF DISPLACEMENT AND MOMENTUM THICKNESS

x/a	Re_a	δ/a	$(\delta_1/a)_d$ (Willmarth's Data)	$(\delta_1/a)_c$ (Computed)	% Error in δ_1 +	$(\theta_1/a)_d$ (Willmarth's Data)	$(\theta_1/a)_c$ (Computed)	% Error in θ_1 †
3514	4330	16.2	6.025	5.666	5.96	5.444	5.250	3.56
1757	6203	10.42	3.689	3.461	6.18	3.120	3.123	0.096
1757	9494	9.45	2.968	2.894	2.49	2.667	2.60	2.51
1757	11693	9.32	2.594	2.760	6.40	2.311	2.496	8.01
878.4	12790	5.52	1.292	1.483	14.78	1.116	1.245	11.56
878.4	19230	4.71	0.981	1.099	12.03	0.827	0.893	7.98
878.4	23100	4.64	0.976	1.051	7.68	0.806	0.855	6.08
439.2	36680	4.12	0.952	1.166	22.48	0.793	0.986	24.34
219.6	74260	1.76	0.315	0.332	5.40	0.265	0.1884	28.91
219.6	92310	1.88	0.337	0.375	11.28	0.261	0.238	8.81

+ $\left|\frac{(\delta_1)_d - (\delta_1)_c}{(\delta_1)_d}\right|$ † $\left|\frac{(\theta_1)_d - (\theta_1)_c}{(\theta_1)_d}\right|$

CHAPTER 4

CONCLUSIONS

(1) For a thick, axisymmetric, turbulent boundary layer on a circular cylinder forms of two similarity laws, one a law of the wall, the other a velocity-defect law have been derived.

(2) In the region of the law-of-the-wall, the logarithmic mixing length is a better approximation than the linear one for the Reynolds stresses for thick, axisymmetric turbulent flows. With this logarithmic mixing length, the mean-velocity distribution, expressed as an integral, Eq. (34), or by an approximation to it which yields a logarithmic law in terms of the exponential integral, Eqs. (42) and (45) shows excellent agreement with the data. Eq. (45) is recommended as a simple, analytical representation of the law of the wall for the thick, axisymmetric, turbulent boundary layers.

(3) The frictional Reynolds number based on cylinder radius, a^*, is an important parameter in the law-of-the-wall region. For large values of a^*, the law-of-the-wall approaches the classical two-dimensional form.

(4) Even for the intermediate values of a^*, in the region where $y^*/a^* \leq 1$, the argument of the logarithmic law

$Y^* = a^* \sqrt{1 + y^*/a^*}\ \ln(1 + y^*/a^*)$ behaves like y^*. Therefore, the Preston-tube technique can be used to measure the wall-shear stress in a thick boundary layer, with the usual calibration curve, as was assumed by Willmarth et al [18].

(5) The axial length scale, $\xi^2 = \frac{x/a}{Re_a}$, of the thick axisymmetric, laminar boundary layer is also a proper scale for correlating a thick, turbulent boundary layer. With this scale, the boundary-layer thickness is well-correlated as power law for a wide range of values of δ/a, x/a and Re_a.

(6) A velocity-defect law, in separable form $\bar{u}_d = \chi(\xi)\ f(\eta)$, has been obtained. This similarity assumption yields the nondimensional velocity defect, $\bar{u}_d = CR^{2(1-b)}\ f(\eta)$. This result shows that the velocity-defect profiles depend strongly on δ/a, as indicated by Willmarth et al [18].

(7) The eddy-viscosity concept for the velocity-defect region appears to be preferable to that of mixing length, but the form of the eddy viscosity needs verification by turbulent-stress measurements. The eddy-viscosity model, in conjunction with similarity, gives the velocity defect in terms of particular confluent hypergeometric functions known as Kummer functions. The mixing-length model, on the other hand, leads to a nonlinear differential equation, the solution of which is a semi-convergent infinite series.

(8) The wake portion of the boundary layer increases as δ/a becomes larger and the wall region decreases correspondingly. Approximately 1/8-th of the boundary layer obeys the law of the wall.

(9) The two similarity laws do not overlap. However, they intersect at about $\frac{y}{\delta + a} = 0.125$. Boundary-layer characteristics computed by using this intersection point agree with the data within an acceptable range of error.

(10) There is insufficient data at large values of δ/a, for a variety of situations, to verify the accuracy of the velocity-defect law obtained in Chapter 2. As stated by Willmarth et al [18],

> "In the future we may gain enough knowledge of the effects of transverse curvature to consider the possibility of creating an empirical formulation for the mean flow in an axisymmetric boundary layer. This was only possible in the two-dimensional case after sufficient data and understanding had accumulated, ..."

In the present work, such a formulation has been proposed, but, in view of the paucity of the available data, it may be necessary in the future to modify the values of the constants when additional data become available.

REFERENCES

[1] Seban, R. A., and Bond, R., "Skin Friction and Heat Transfer Characteristics of a Laminar Boundary Layer on a Cylinder in Axial Incompressible Flow," Journal of Aeronautical Sciences, Vol. 18, 1952.

[2] Kelly, H. R., "A Note on the Laminar Boundary Layer on a Circular Cylinder in Axial Incompressible Flow," Journal of Aeronautical Sciences, Vol. 21, 1954.

[3] Glauert, M. B., and Lighthill, M. J., "The Axisymmetric Boundary Layer on a Long Thin Cylinder," Proceedings of the Royal Society, London, Vol. 230, 1955.

[4] Landweber, L., "Effect of Transverse Curvature on Frictional Resistance," David Taylor Model Basin Report No. 689, 1949.

[5] Richmond, R., "Experimental Investigation of Thick Axially Symmetric Boundary Layers on Cylinder at Subsonic and Hypersonic Speeds," Ph.D. thesis, California Institute of Technology, Pasadena, Ca., 1957.

[6] Rao, G.N.V., "The Law of the Wall in a Thick Axisymmetric Turbulent Boundary Layer," Journal of Basic Engineering, Trans. ASME, Series D, Vol. 89, No. 1, March 1967, pp. 237-238.

[7] Rao, G.N.V., and Keshavan, N. R., "Axisymmetric Turbulent Boundary Layers in Zero Pressure Gradient Flows," Journal of Applied Mechanics, Trans. ASME, Vol. 94, 1972, p. 25.

[8] Yu, Y. S., "Effects of Transverse Curvature on Turbulent Boundary Layer Characteristics," Journal of Ship Research, Vol. 3, 1958, p. 33.

[9] Chin, Y. T., Hulesbos, J., and Hunnicutt, G. H., "Effect of Lateral Curvature on the Characteristics and Skin Friction on a Turbulent Air Boundary Layer, With or Without Helium Addition," Proceedings, Heat Transfer and Fluid Mechanics Institute, 1967.

[10] Sparrow, E. M., Eckert, E.R.G., and Minkowycz, W. J., "Heat Transfer and Skin Friction for Turbulent Boundary Layer Flow Longitudinal to a Circular Cylinder," Journal of Applied Mechanics, Vol. 30, 1963, p. 37.

[11] Patel, V. C., "A Unified View of the Law of the Wall Using Mixing-Length Theory," Iowa Institute of Hydraulic Research, Report No. 137, 1972.

[12] Landweber, L., and Poreh, M., "Frictional Resistance of Flat Plates in Dilute Polymer Solutions," Journal of Ship Research, Vol. 17, No. 4, 1973, pp. 227-240.

[13] White, F. M., "An Analysis of Axisymmetric Turbulent Flow Past a Long Cylinder," Journal of Basic Engineering, Trans. ASME, Vol. 94, 1972, p. 200.

[14] Cebeci, T., "Laminar and Turbulent Incompressible Boundary Layers on Slender Bodies of Revolution in Axial Flow," Journal of Basic Engineering, Trans. ASME, Series D, Vol. 92, p. 545.

[15] Afzal, N., and Narasimha, R., "Axisymmetric Turbulent Boundary Layer Along a Circular Cylinder at Constant Pressure," Journal of Fluid Mechanics, Vol. 74, 1976, p. 113.

[16] Yasuhara, M., "Experiments of Axisymmetric Boundary Layers Along a Cylinder in Incompressible Flow," Transactions of the Japan Society of Aerospace Sciences, Vol. 2, 1959, p. 33.

[17] Willmarth, W. W., and Yang, C. S., "Wall-Pressure Fluctuations Beneath Turbulent Boundary Layers on a Flat Plate and a Cylinder," Journal of Fluid Mechanics, Vol. 41, p. 47.

[18] Willmarth, W. W., Winkél, R. E., Bogar, T. J., and Sharma, L. K., "Axially Symmetric Turbulent Boundary Layers on Cylinders: Mean Velocity Profiles and Wall Pressure Fluctuations," The University of Michigan, Department of Aerospace Engineering Gas Dynamics Laboratories, 1975.

[19] Afzal, N., and Singh, K. P., "Measurements in an Axisymmetric Turbulent Boundary Layer Along a Circular Cylinder," Aeronautical Quarterly, Vol. 27, 1976, p. 217.

[20] Patel, V. C., Nakayama, A., and Damian, R., "An Experimental Study of the Thick Turbulent Boundary Layer Near the Tail of a Body of Revolution," Iowa Institute of Hydraulic Research, Report No. 142, 1973.

[21] Abramowitz, M., and Stegun, I.A., "Handbook of Mathematical Functions," Dover Publications, Inc., New York, 1970.

[22] Magnus, W., Oberhettinger, F., and Soni, R.P., "Formulas and Theorems for the Special Functions of Mathematical Physics." Springer-Verlag, New York Inc., 1966.

APPENDIX

SOME PROPERTIES OF KUMMER FUNCTION U(b,c,z)[†]

The following properties of the Kummer function, U(b,c,z), were applied in the text and were required in numerical evaluations.

(1) $$\frac{d^n}{dz^n}\left[e^{-z}\, U(b,c,z)\right] = (-1)^n\, e^{-z}\, U(b,c+n,z)$$

(2) $$\int e^{-z}\, z^{c-1}\, U(b,c,z)\,dz = -e^{-z}\, z^{c}\, U(b+1,c+1,z)$$

(3) $$(b+z)\, U(b,c,z) + b(c-b-1)\, U(b+1,c,z) - zU(b,c+1,z) = 0$$

[†]Magnus et al. [22]